Fermilab T1044 Beam Characterization with Lead Glass Calorimeter

Francesco Vassalli

November 28, 2018

Abstract

This analysis note summarizes the 2018 test beam linearity and resolution characterization of the Fermilab Test Beam. A Lead Glass (PbGl) calorimeter is used in series with Cherenkov, hodoscope, and veto counters which isolate single electron events. The measured versus predicted test beam momentum agrees with linear scaling, and no momentum correction is needed to calibration of the sPHENIX calorimeters. This agrees with past results [2]. The resolution is $\frac{(6.4\pm.3)\%}{\sqrt{E}} \oplus (1.9 \pm .1)\%$. This is significantly worse resolution than past results most likely due to low statistics and high beam spread at low energy. The constant term represents the beam spread which agrees with past results [3][2].

Contents

Chapter 1

Introduction

This analysis uses a lead glass calorimeter (PbGl) to characterize the Fermilab Test Beam. A series of cuts to isolate good ADC PbGl signal. The signal for a range of test beam momentum and photomultipler voltages are fit to Gaussians. These fits are used to characterize the test beam momentum linearity and momentum spread.

1.1 Detector Setup

1.1.1 Overview

The analysis uses the three detectors described in section 1.1.2 to make cuts on the events and measures each event with analog digital converted (ADC) signal from the PbGl. Good events are single electrons that travel directly through the PbGl.
A total of 43 runs were used in this analysis. Each run has a designated run number, signal for each hodoscope, veto counter, Cherenkov counter, PbGl signal, predicted beam momentum, and voltage across the PbGl photomultipliers. The data was taken at two different times with the first set in late February and the second set in May of 2018. All the data has had the electronic pedestal removed before this analysis. The first step of the analysis was to determine which runs had good signal. All the runs with beam momentum and voltage that do not correspond to table 1.1 were discarded for having too little data or signal saturation. The runs where the beam momentum is too low for the photomultiplier voltage have too little data to make a good fit. The runs with beam momentum too high for the photomultiplier voltage have more signal than the amplifier can create indicating the readout ADC is saturated. In the appendix is a list of every run. The runs that were not included have a reason listed.

1.1.2 Cuts

The PbGl signal was isolated in each run based off cuts from the signal in the Cherenkov, hodoscope, and veto counters. A good event is defined to have positive Cherenkov signal, exactly one hit in the horizontal hodoscope layer, exactly one hit in the vertical hodoscope layer, and no veto hits.

- Lead Glass Calorimeter- records the energy of each event which is the main observable for the analysis.

Predicted Beam Energy	PbGl Voltage
2-8	1200
4-16	1100
20-28	1000

Table 1.1: Voltage used for each predicted beam energy. Note the overlap between 1200 and 1100V.

- Cherenkov Counter - the beam particles pass through a gas which is pressure controlled to select the speed of light in the gas. Particles travelling faster than the speed of the light emit Cherenkov radiation which transmitted as signal. This allows a beam of particles travelling with the same

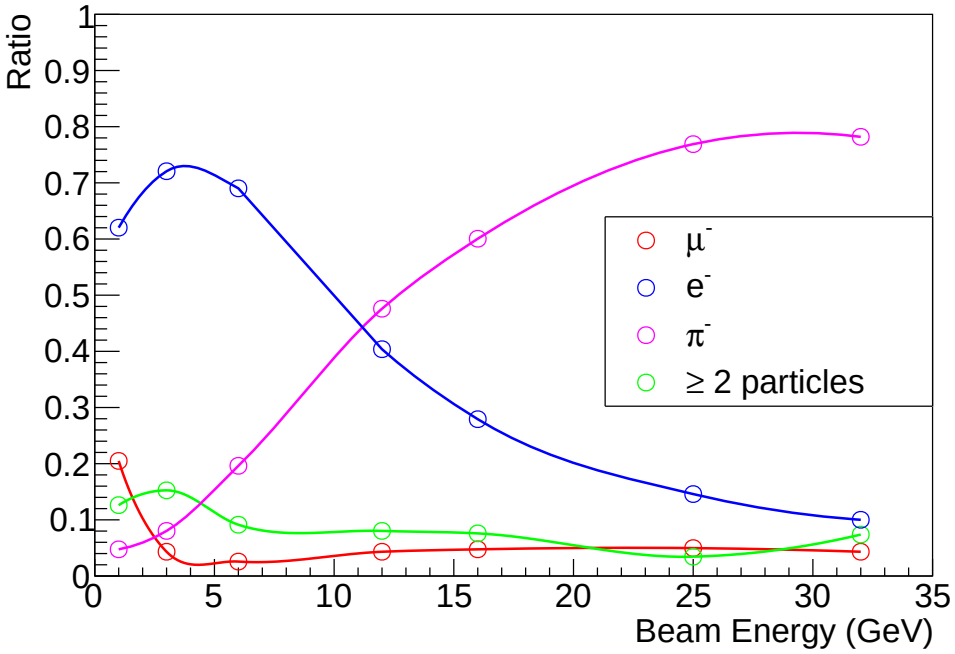

Figure 1.1: The relative abundance of particle species present in the negatively charged Fermilab Test Beam as a function of beam energy.[1]

momentum to be selected by their velocity [1]. The Cherenkov cut is used on all the events with a predicted beam energy of less than 20. An ADC signal of greater than 1400 was chosen to be the cutoff for what is considered a good hit in the Cherenkov. This was visually determined by plotting the Cherenkov signal for each run. At greater than or equal to 20GeV the Cherenkov

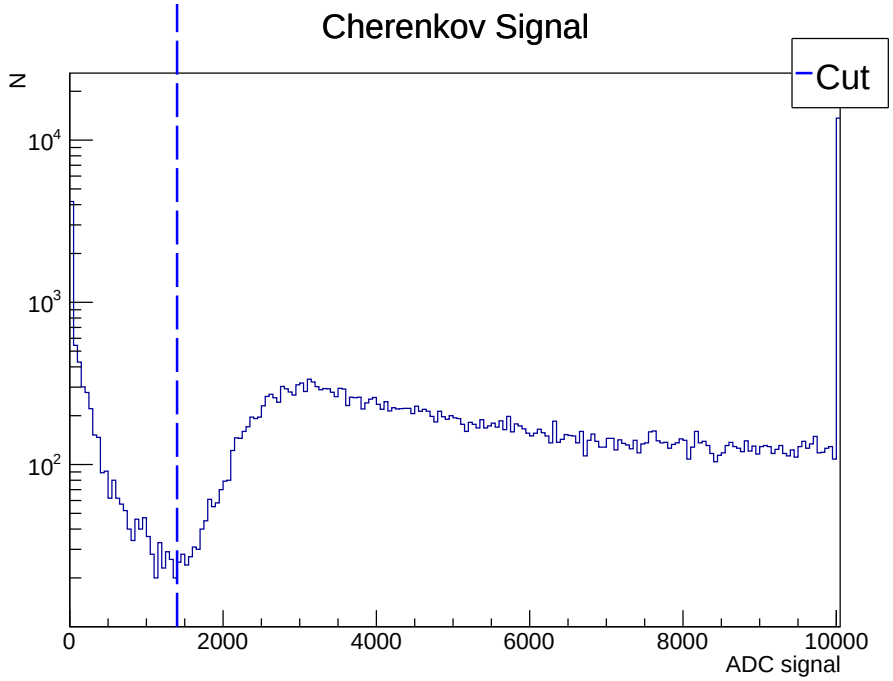

Figure 1.2: Example of Cherenkov signal run 558 predicted beam energy 2GeV 1200V.

counter does not have good signal. The cut is substituted for a Gaussian background model which is used to isolate the beam electron peak from π^- nuclear interaction with the calorimeter.

- Hodoscope - the beam passes through two sets of hodoscopes one vertical and one horizontal.

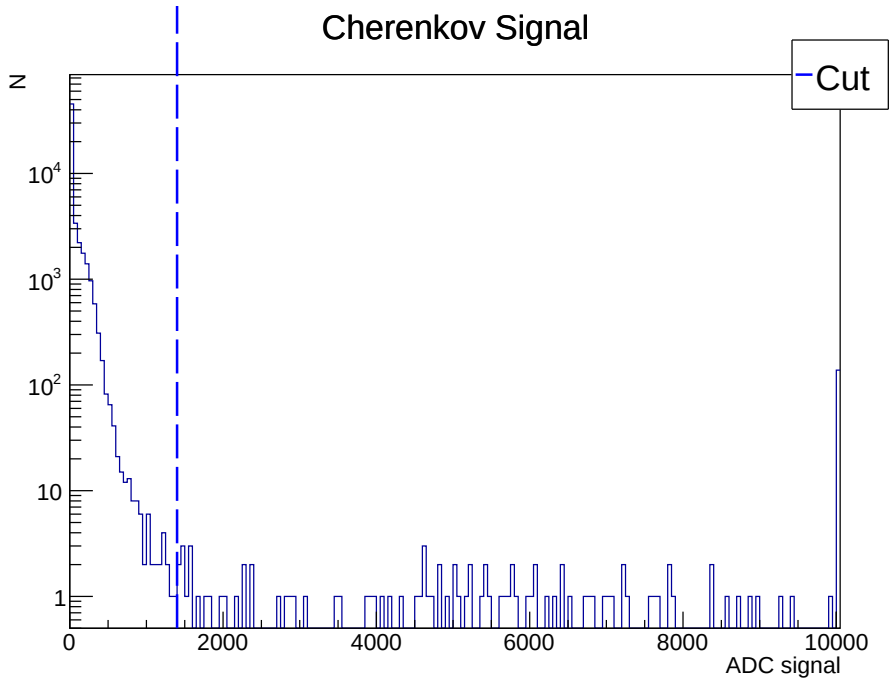

Figure 1.3: Example of Cherenkov signal run 1943 predicted beam energy 20GeV 1000V. Demonstrates why the Cherenkov signal is not used as a cut past 20GeV.

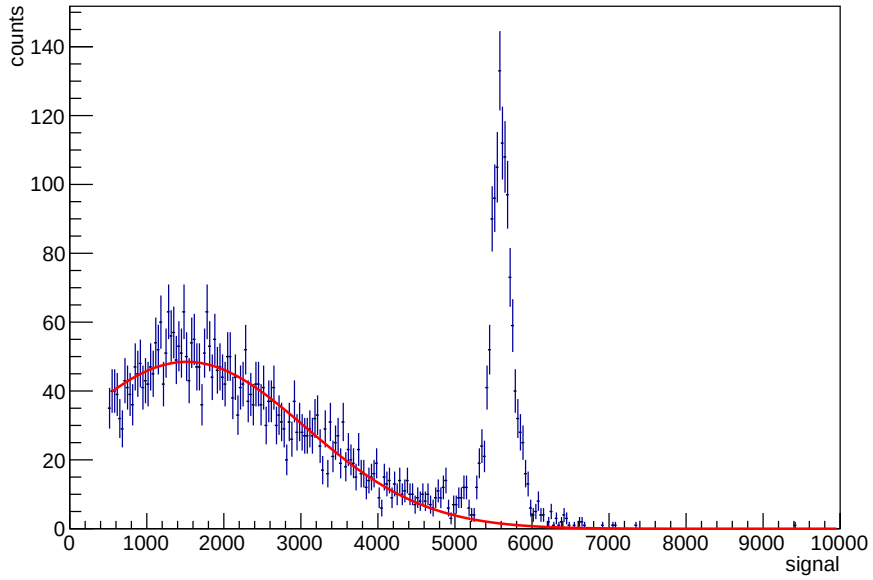

Figure 1.4: Example of Gaussian background model to PbGl signal run 1943. This fit is subtracted from the data instead of using the Cherenkov counter. Demonstrates how the signal is isolated from π^- nuclear interaction without the Cherenkov cut. A new Gaussian is fit to the signal peak. In the appendix is an example of the same process with a exponential fit the measurement for this process agrees within uncertainty.

Each event is required to have exactly one hit in the vertical set of hodoscopes and 1 hit in the horizontal set. There are 8 hodoscopes in either direction forming a 64 cell grid. This ensures that each good event has only one particle[2]. Only the center 4 hodoscopes in each direction are used. This 16 cell grid is a tighter cut than the 8x8. Ideally a 2x2 cut should be used, but applying a 2x2 cut in this analysis left too few points in the low energy runs to precisely fit a Gaussian to the PbGl

signal. The hodoscope cuts were determined in a similar manner to the Cherenkov signal. Each hodoscope independently received a cut.

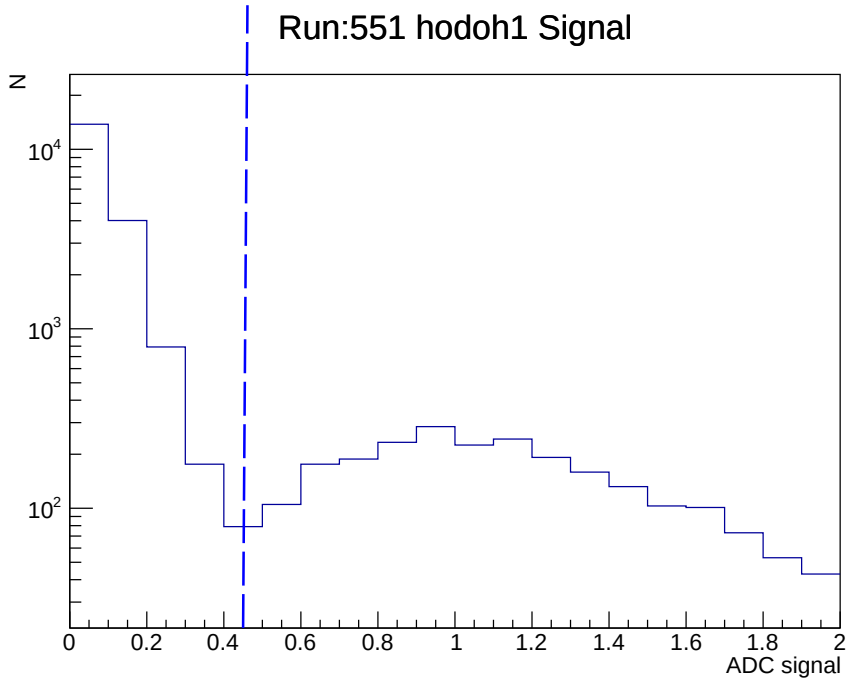

Figure 1.5: Example of hodoscope cut with signal from horizontal hodoscope 1. Events above the line are considered hits. Run 551 4GeV 1200V

- Veto counter- Four veto counters were placed around the beam path. Any event with a veto signal is rejected this ensures that good event only records particles travelling directly in the beam direction. All the veto counters were given the same veto cut. In May data set, it appears that the 4th veto counter was calibrated slightly differently, so a new cut was made for that veto counter in the corresponding runs.

1.2 Hodoscope Analysis of Beam Position

The 8 vertical and 8 horizontal hodoscopes make a 64 cell grid for the beam to pass through. By plotting the index of each hodoscope that is triggered in an event one can make a picture of the beam position.

The hodoscope picture for this test shows that at low energy the beam is spread over the whole 8x8 grid while at mid and high energy the beam is focused. The beam spread at low energy may contribute to low resolution.

Possible leakage contribution to the resolution was investigated by comparing the resolution of the PbGl signal in mid and high energy runs with a 4x4 hodoscope cut excluding events with 2x2 hodoscope hits to 2x2 hodoscope cut. It is not possible to do the same at low energy due to too few statistics in the 2x2 cut. The resolution for the 4x4 excluding 2x2 cuts agrees with the 2x2 cut which demonstrates there is little leakage.

1.3 Observable

The main observable for this analysis is the ADC signal from the PbGl. The ADC signal for every event is recorded and a Gaussian is fit to the data. The mean (μ) of each Gaussian is used to create a plot PbGl response with respect to predicted beam energy. This is referred to as linearity and is presented in chapter 2. The σ of the Gaussian is divided by μ and is referred to as resolution. The resolution is plotted with respect to beam energy to find the stochastic equation and presented in chapter 3. The uncertainty in σ is reported directly from the ROOT fitting algorithm. The mean uncertainty is the mean uncertainty of the fitting algorithm added in quadrature with the bin width uncertainty.

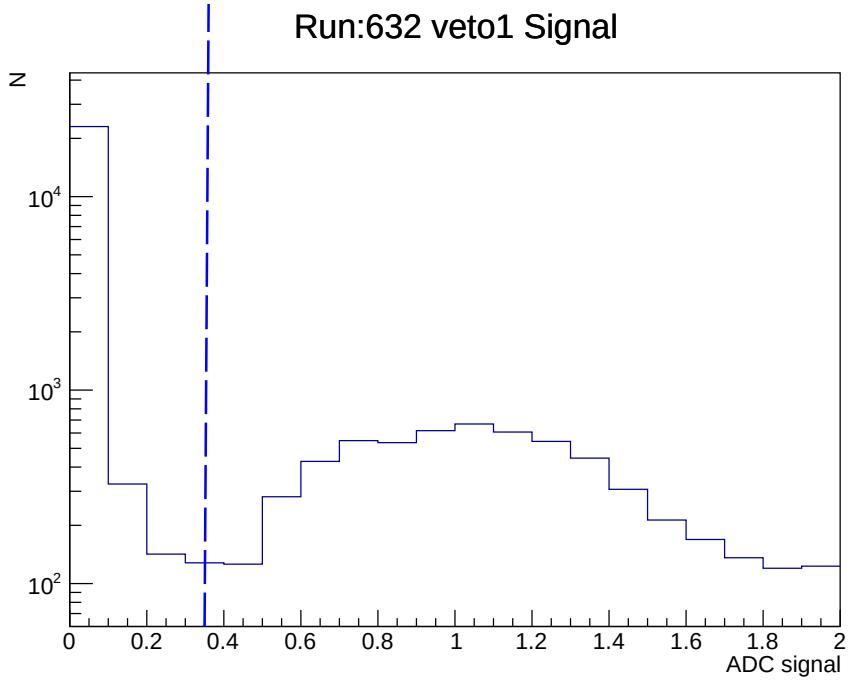

Figure 1.6: Example of veto cut with signal from veto counter 1. Events below the line are considered hits. Run 632 12GeV 1100V.

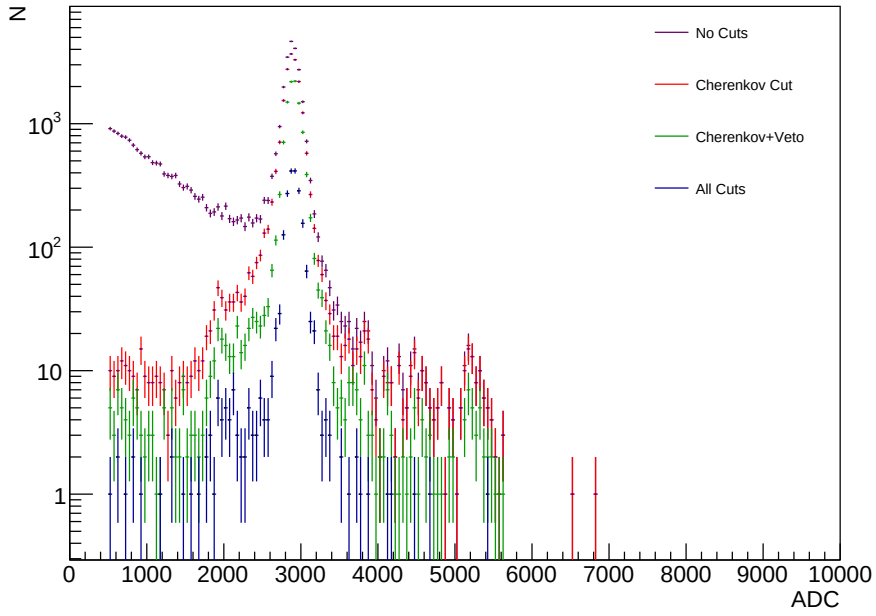

Figure 1.7: Example of the cut regimen for run 632 12GeV 1100V.

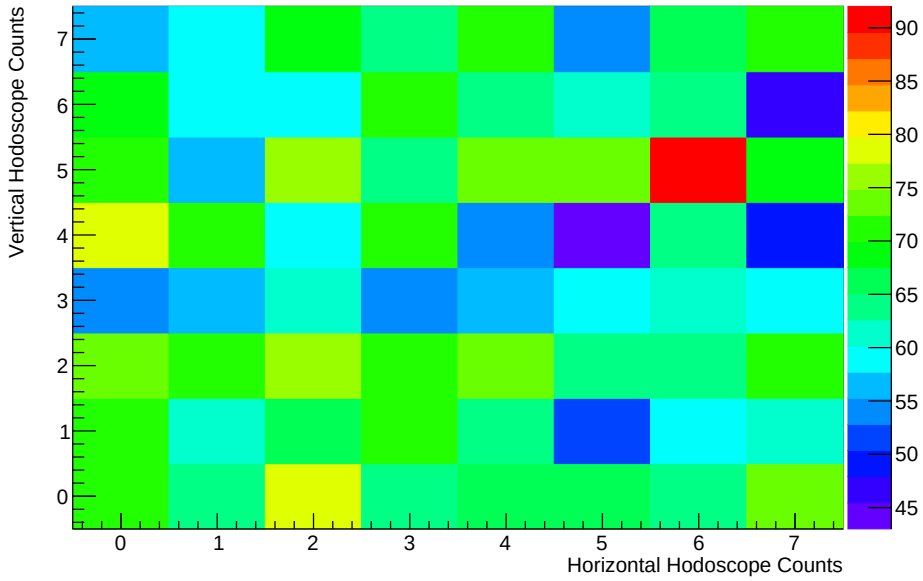

Figure 1.8: Example of the 8x8 hodoscope map for for run 2045 2GeV 1200V. This demonstrates a typical beam spread at low energy.

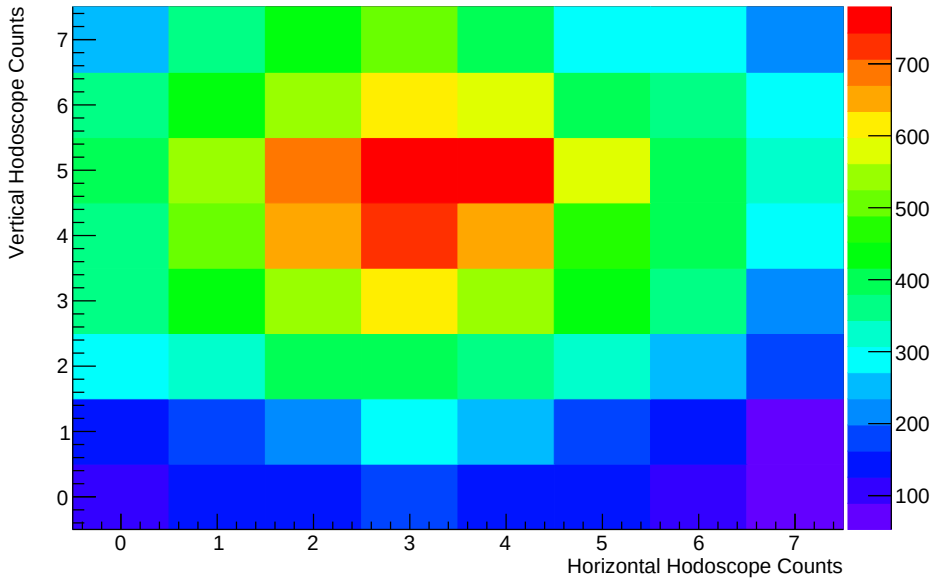

Figure 1.9: Example of the 8x8 hodoscope map for for run 2126 12GeV 1100V. This demonstrates a typical beam spread at mid energy.

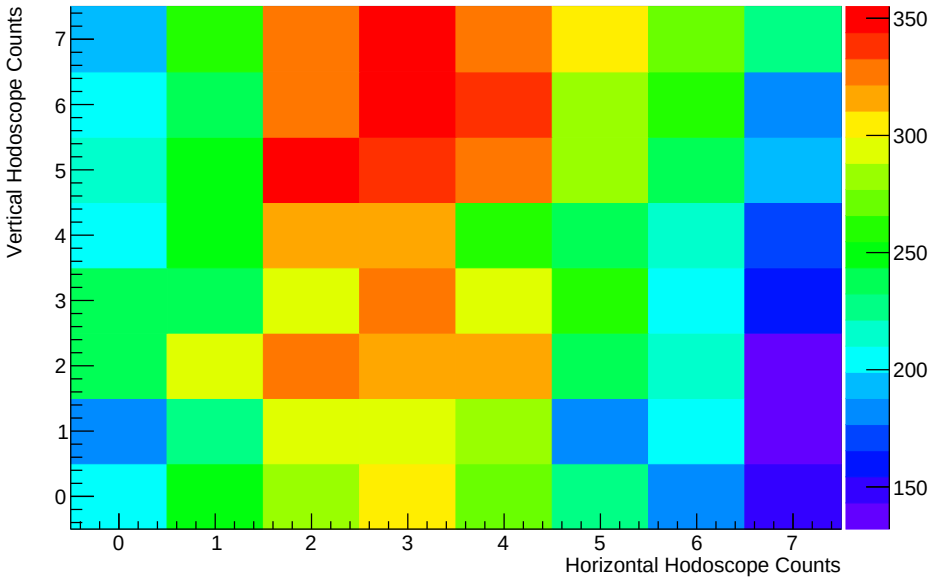

Figure 1.10: Example of the 8x8 hodoscope map for for run 2167 28GeV 1000V. This demonstrates a typical beam spread at high energy.

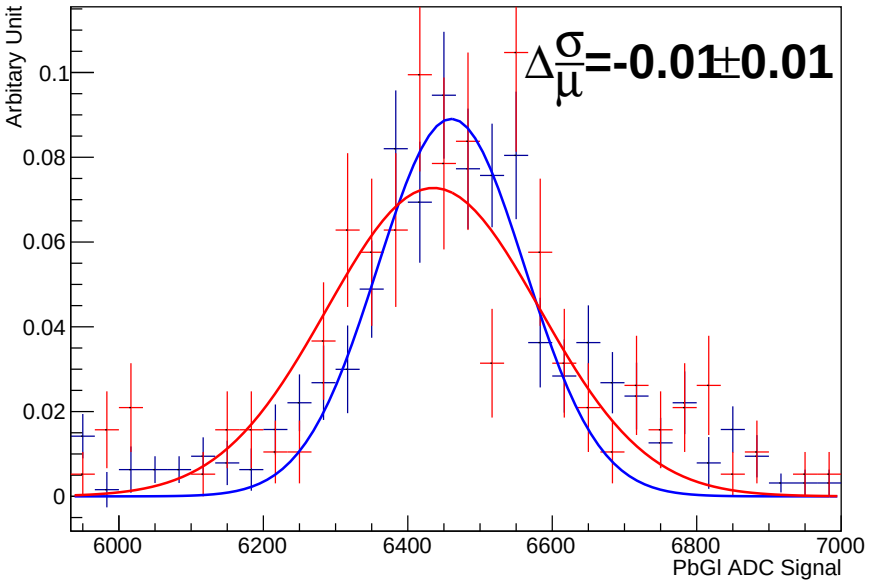

Figure 1.11: Example of comparing the 4x4 excluding 2x2 cut to the 2x2 cut. The PbGl signal is normalized to 1 in both plots and their difference in resolution is displayed. The uncertainty on the difference is 100%. Run 1945 1000V 28GeV.

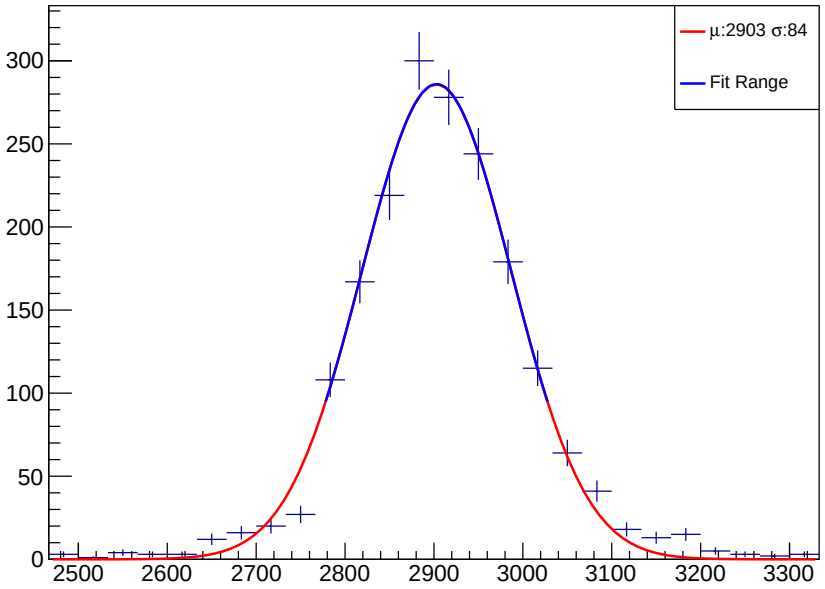

Figure 1.12: Example of PbGl signal with the Gaussian fit and the range it is fit over. Run 632 12GeV 1100V.

Chapter 2

Linearity of Test Beam

2.1 Introduction

Linearity is the ratio between the momentum of particles at the calorimeter and the selected momentum of the beam. If the momentum of particles at the calorimeter did not scale linearly with beam input energy due to problems with the test set up, then the momentum characterization of the PbGl can be used to derive corrective factors. In the calibration of the sPHENIX calorimeters, these corrective factors can be used to correct the beam momentum. However this analysis reports the momentum of beam particles as measured by the PbGl scales within less than one σ.
First the conversion factors are derived to relate the ADC signal to units of beam momentum [GeV]. Then each run is plotted in terms of measured beam momentum with respect to predicted beam momentum and fit the data to line. The slope of this line is called the linearity.

2.2 ADC to GeV Conversion

The data from the PbGl is reported in terms of analog digital converted signal. It comes in five sets. There are two sets from February at 1100V and 1200V respectively, and there are three sets from May at 1000, 1100, and 1200 volts. The 1000V data from February is not used because there were not enough point to derive a conversion factor. Separate conversion factors are derived for each data set. The mean of each Gaussian within a data set is plotted with respect to the predicted beam momentum and fit to a line which is used to convert to measured GeV. Note that runs with same beam momentum as combined using a weighted sum of their uncertainties.

2.3 Result and Uncertainties

After applying the conversions to each data set the data can be compared between sets. A new linear fit is made to the combined data and the constant term is fixed at zero. The uncertainty on each point is the PbGl uncertainty described in section 1.3 propagated through conversion from ADC signal to GeV. The χ^2 in figure 2.3 is low because of the unit conversion process. Fitting a line for the conversion factors to each data set independently allows few degrees of freedom, therefore, a low χ^2 is expected. All the unconverted linearity plots are included in section 4.2. Each data set is linear independently which matches with the converted result. This also agrees with past analysis [2].

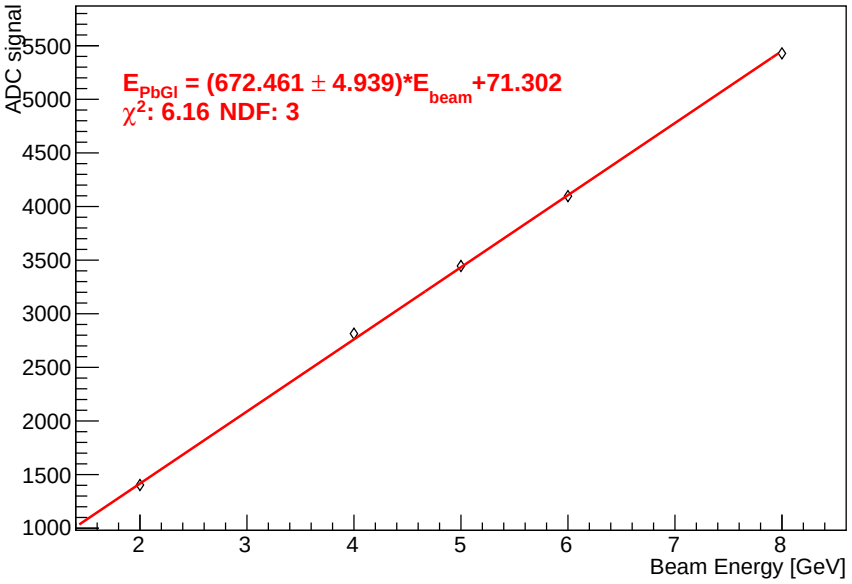

Figure 2.1: ADC signal from the fist set of 1200V runs as a function of predicted beam momentum with a linear fit.

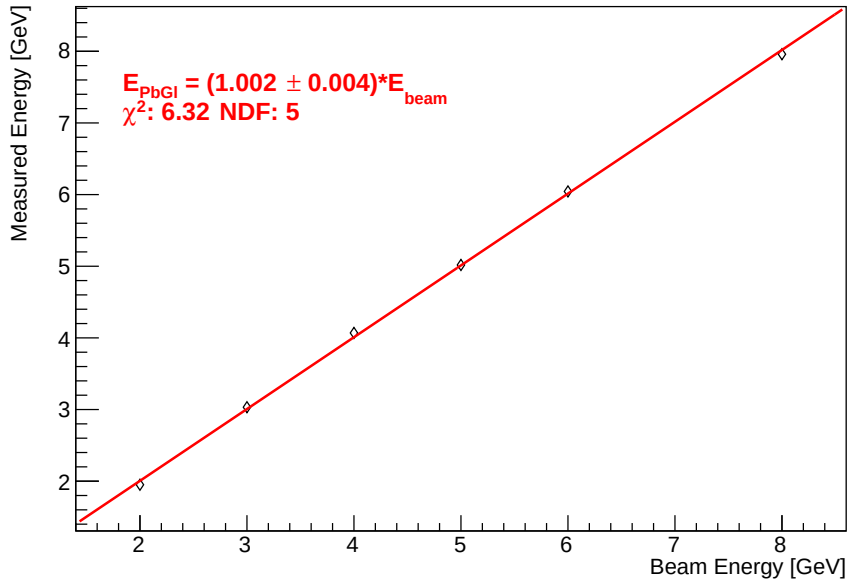

Figure 2.2: The data from figure 2.1 and the second set of 1200V runts after applying the conversion. This converts the y axis from ADC to measured GeV

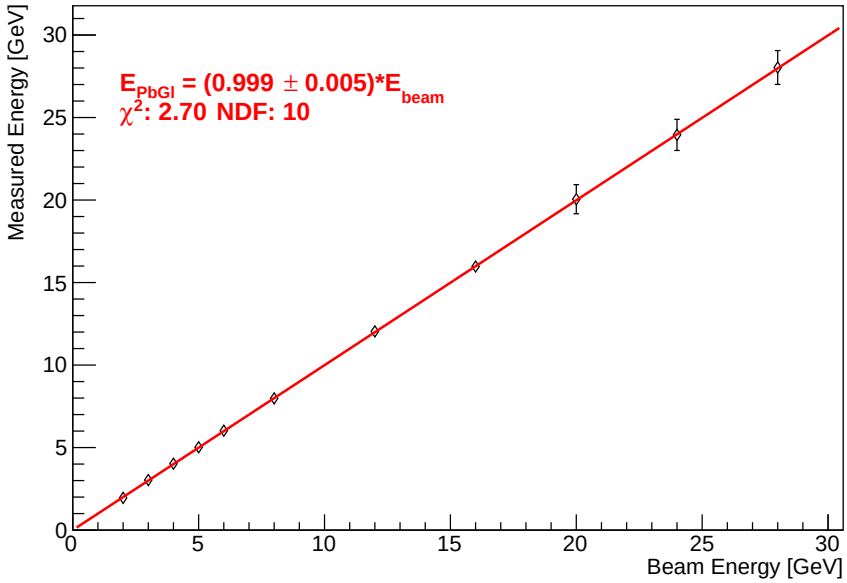

Figure 2.3: Linear fit to all the data. This is the reported linearity of the test beam

Chapter 3

Resolution of the Test Beam

3.1 Introduction

The resolution of is defined by the fit of equation 3.1 to the resolution of each run as a function of predicted beam momentum[4].

$$\frac{A}{\sqrt{E}} \oplus B \tag{3.1}$$

The resolution of each run is defined to be the σ of the Gaussian fit to each PbGl run divided by its mean. There is no unit conversion for the resolution analysis because $\frac{\sigma}{\mu}$ is unitless. This also indicates that all the runs can be directly compared. Runs with the same predicted beam momentum have their resolution averaged in a sum weighted by the resolution uncertainty.

3.2 Result

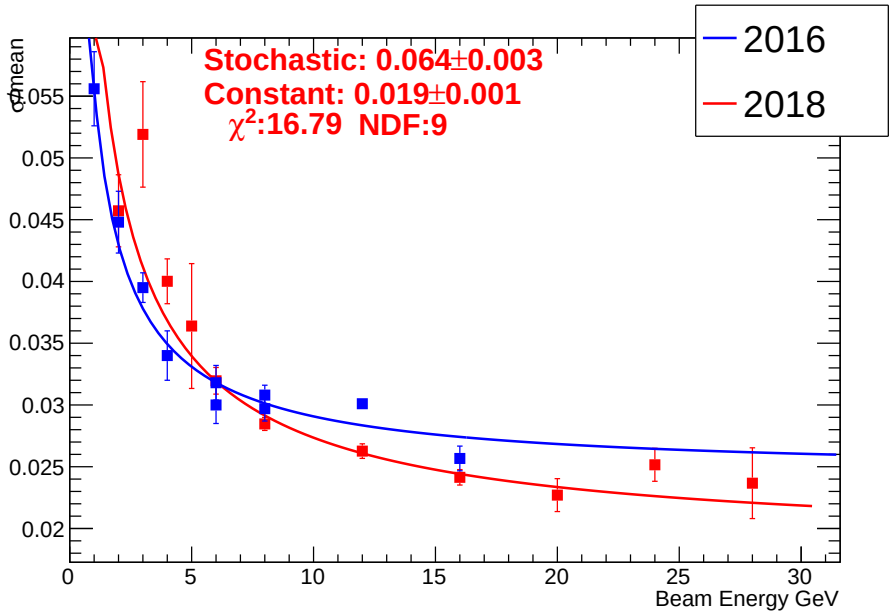

Figure 3.1: The fit of equation 3.1 to the resolution of each run. This is the reported resolution of the test beam. Note the 2016 analysis is interpolated over 1-16 GeV whereas this analysis (Red) is interpolated 2-28GeV

The resolution is $\frac{(6.4\pm.3)\%}{\sqrt{E}} \oplus (1.9 \pm .1)\%$.
The first term disagrees with past analysis which found the resolution is $\frac{5\%}{\sqrt{E}} \oplus 2.4\%$[2]. The beam spread

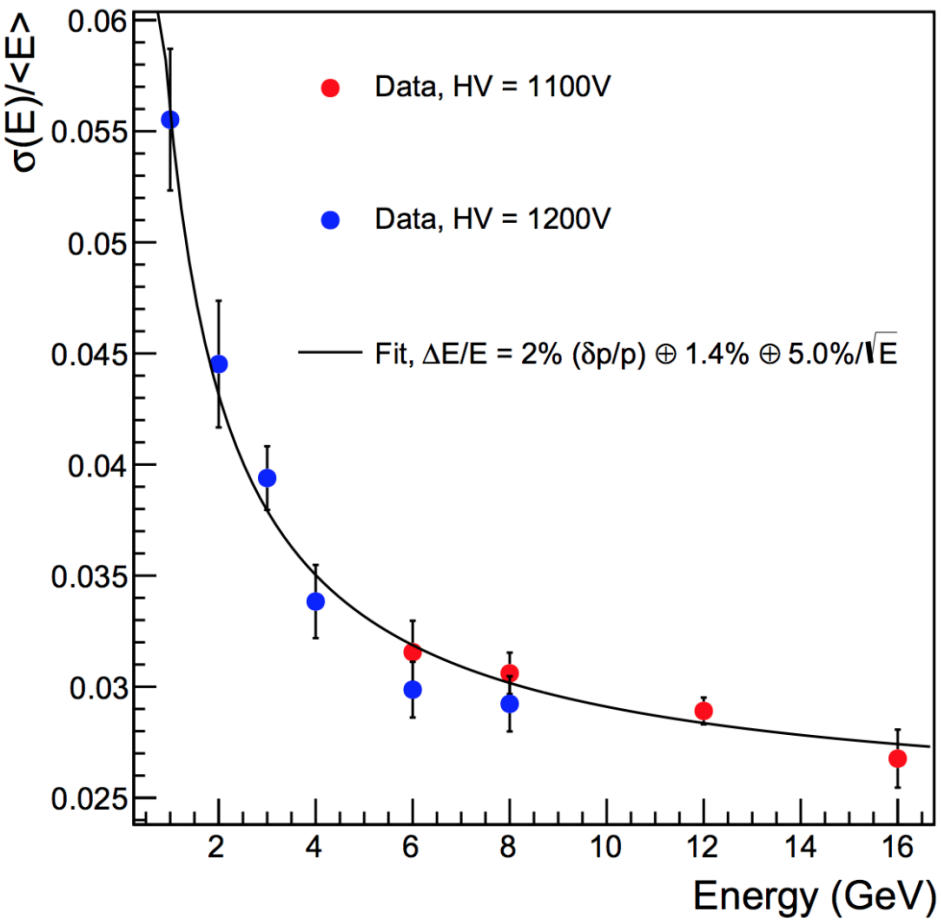

Figure 3.2: The published 2016 resolution.

at low energy and low statistics makes the resolution significantly worse. The 2016 analysis used data with predicted beam momentum 1-16GeV whereas this analysis includes 2-28 GeV[2]. The lack of a 1GeV data point in this analysis is due to too few events in that run. This term captures the statistics related fluctuations and the uncertainty from dead material at the front of the calorimeter [4]. The disagreement between this analysis and 2016 is most likely due to statistics, but the front of the PbGl should be checked for dead material.

The second term agrees with past analysis. It captures the calibration uncertainty, damage and non-uniformity in the detector, and beam momentum spread [4]. There is little non-uniformity or damage to the PbGl. The calibration uncertainty is significantly less than the beam momentum spread. This indicates the constant term is equal to the beam momentum spread which is $(1.9 \pm .1)\%$. This agrees exactly with Fermilab's simulations [3] and agrees with past analysis of the same setup [2].

Chapter 4

Appendix

4.1 Run Catalog

Table 4.1: Each run indicating if it was used or why it was not.

runnumber	energy	included	reason
322	-8	N	
323	-8	N	
328	-8	N	
329	-8	N	
330	-8	N	
331	-8	N	
332	-8	N	
333	-8	N	
334	-8	N	
335	-8	N	
336	-8	N	
337	-8	N	
338	-8	N	
339	-8	N	
499	-8	N	
500	-8	N	
502	-8	N	
544	-8	Y	
545	-8	N	
551	-4	Y	
558	-6	Y	
563	-2	Y	
567	-8	Y	
568	-8	N	saturated
572	-12	N	saturated
573	-12	N	saturated
574	-12	Y	
577	-2	N	undersaturated
578	-2	N	undersaturated
579	-2	N	undersaturated
580	-2	N	undersaturated

runnumber	energy	included	reason
631	-8	Y	
632	-12	Y	
652	-16	Y	
653	-16	N	not enough points
654	-24	N	not enough points
655	-24	N	not enough points
687	-28	N	saturated
772	10	N	beam charge
773	10	N	beam charge
776	-2	Y	
777	-2	Y	
809	-6	Y	
810	-4	Y	
816	-2	Y	
829	-6	Y	
830	-2	Y	
849	-2	Y	
859	-5	Y	
900	-1	N	undersaturated
1876	-8	N	undersaturated
1879	-8	Y	
1882	-8	Y	
1883	-8	Y	
1888	-8	Y	
1889	-6	Y	
1890	-6	Y	
1901	-4	Y	
1902	-4	Y	
1904	-2	N	undersaturated
1906	-2	Y	
1924	-12	N	saturated
1925	-12	Y	
1926	-16	Y	
1943	-24	Y	
1945	-28	Y	
2045	-2	Y	
2073	-3	Y	
2074	-4	Y	
2094	-6	Y	
2095	-6	Y	
2097	-8	Y	
2098	-8	Y	
2125	-12	N	saturated
2126	-12	Y	
2127	-16	Y	
2128	-16	N	saturated
2149	-20	Y	
2150	-24	Y	
2167	-28	Y	

4.2 Unconverted Linearity

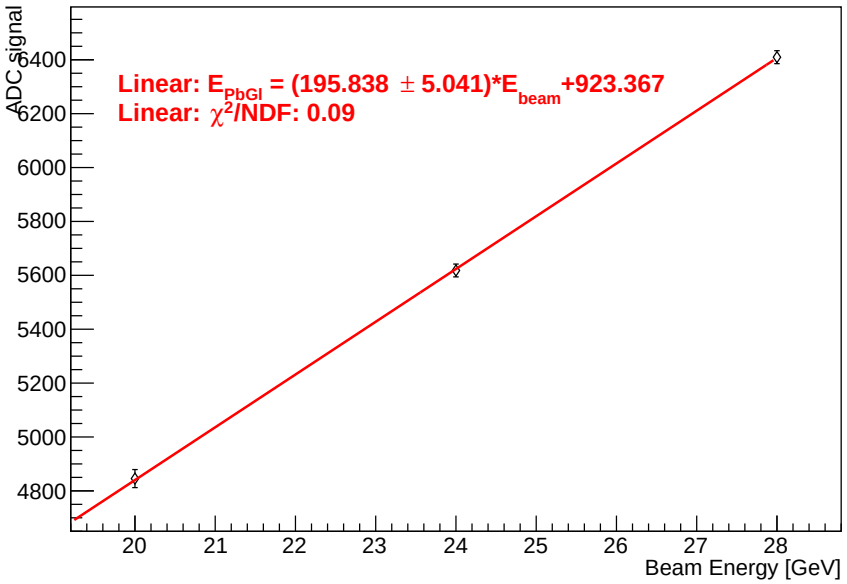

Figure 4.1: The unconverted linearity for the set of 1000V runs

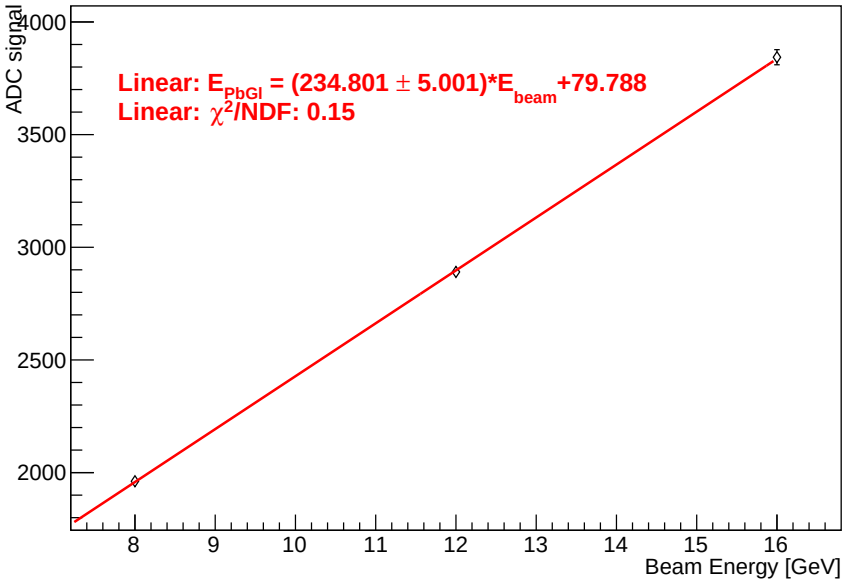

Figure 4.2: The unconverted linearity for the first set of 1100V runs

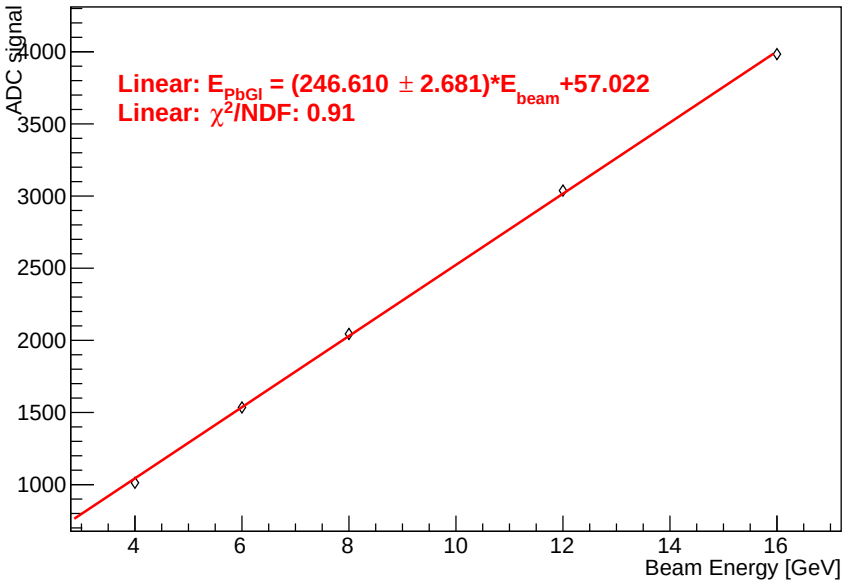

Figure 4.3: The unconverted linearity for the second set of 1100V runs

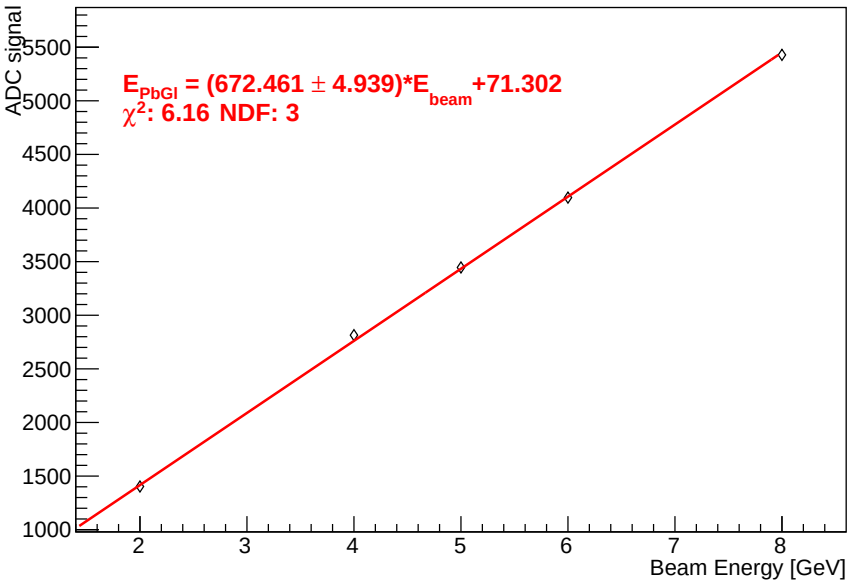

Figure 4.4: The unconverted linearity for the first set of 1200V runs

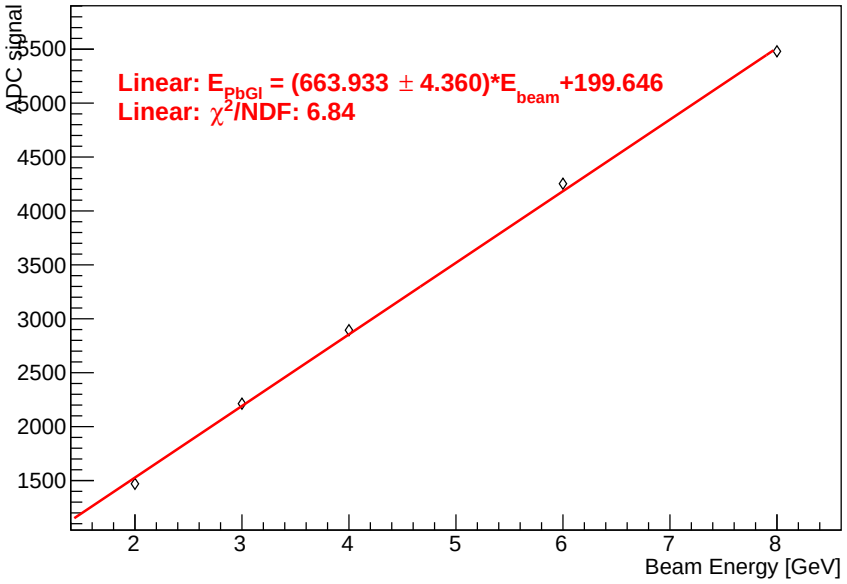

Figure 4.5: The unconverted linearity for the second set of 1200V runs

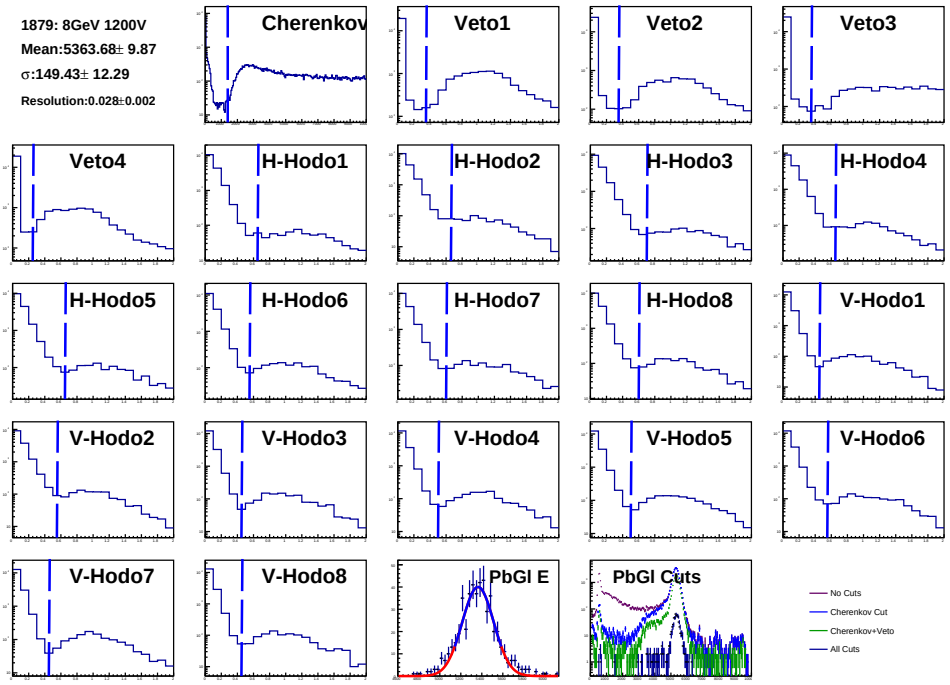

8GeV 1200V.pdf

4.3 Summary For Each Run

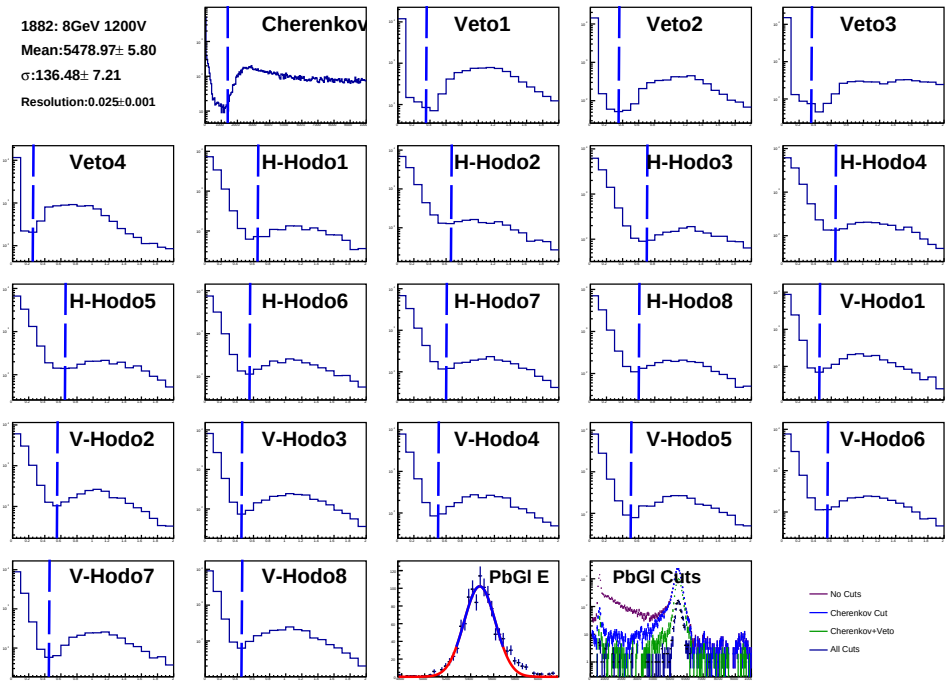

8GeV 1200V.pdf

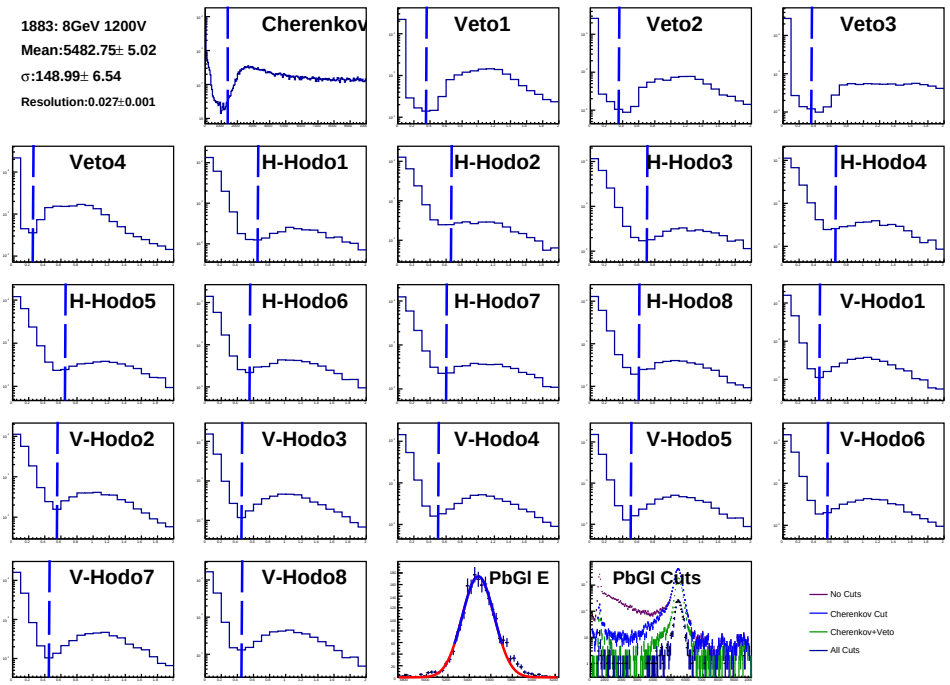

8GeV 1200V.pdf

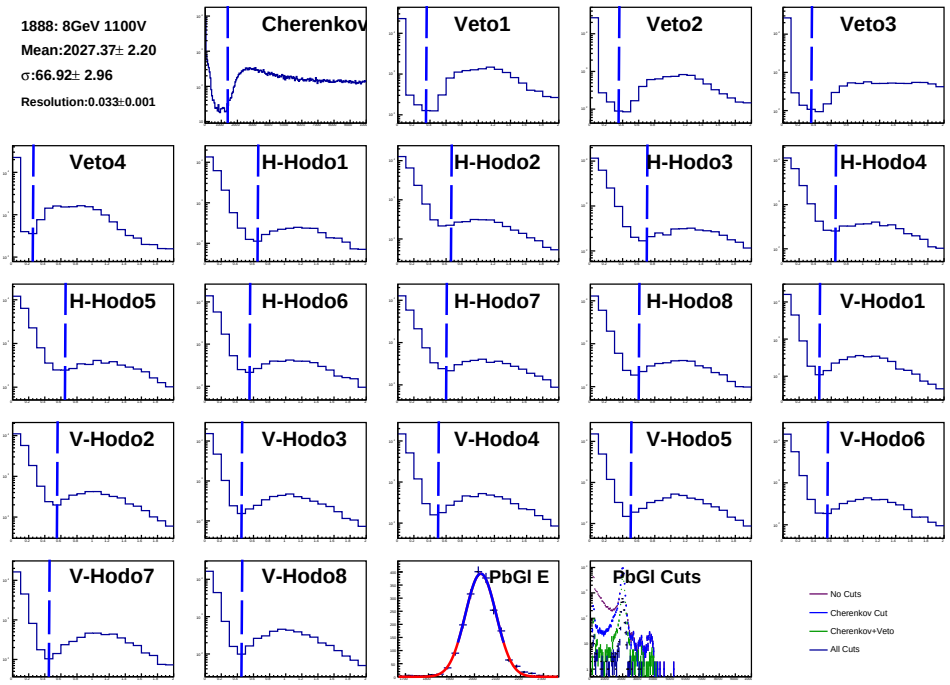

8GeV 1100V.pdf

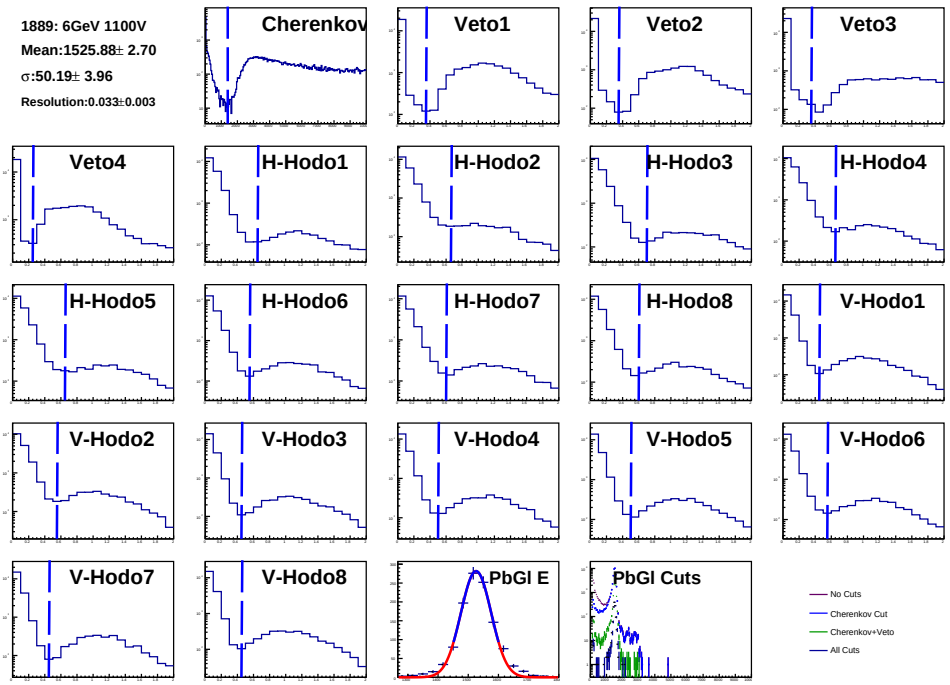

6GeV 1100V.pdf

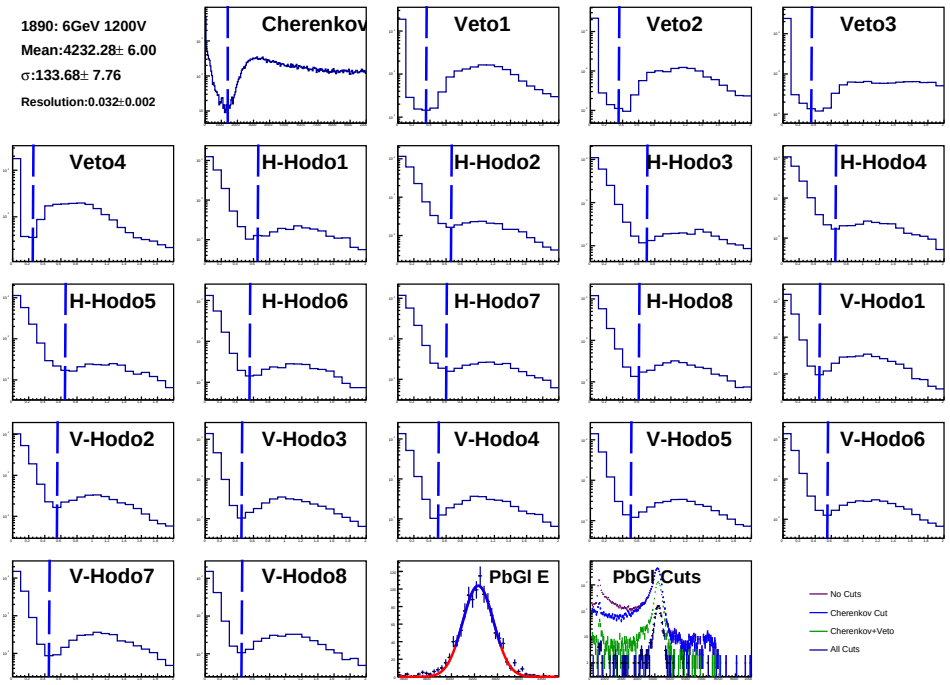

6GeV 1200V.pdf

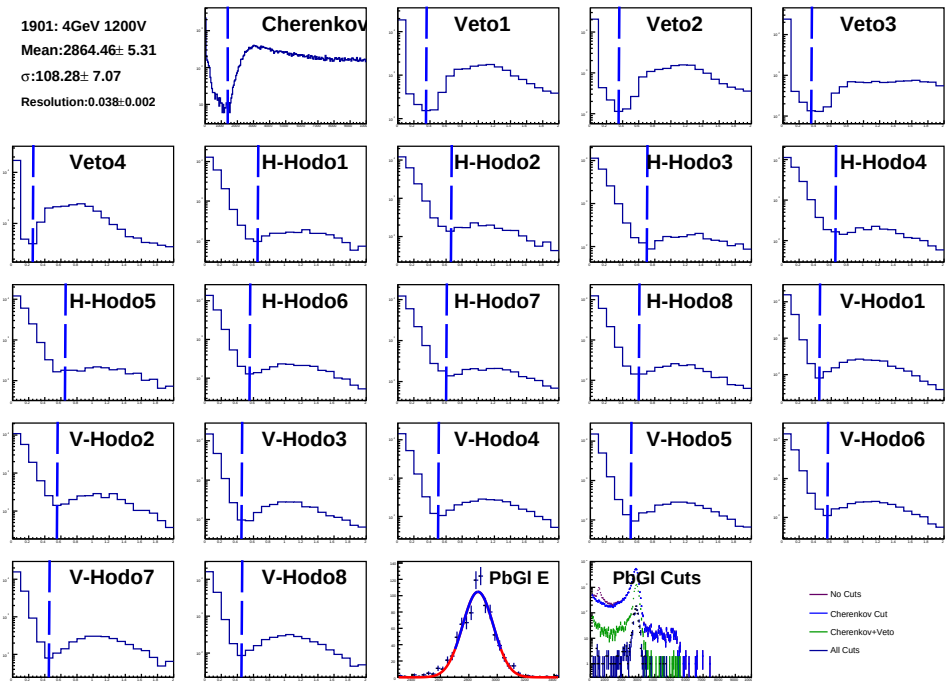

4GeV 1200V.pdf

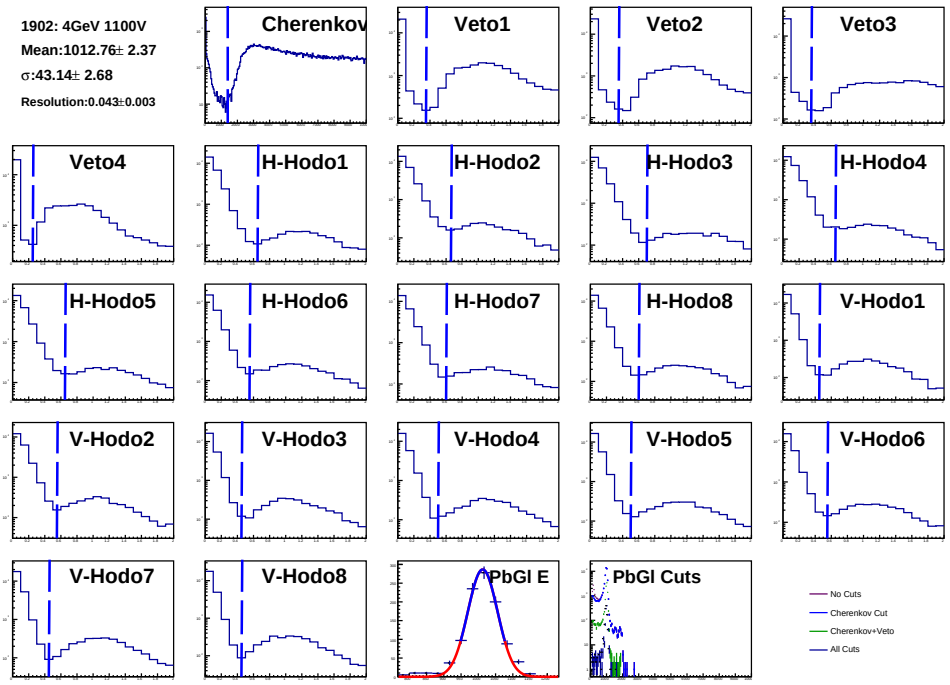

4GeV 1100V.pdf

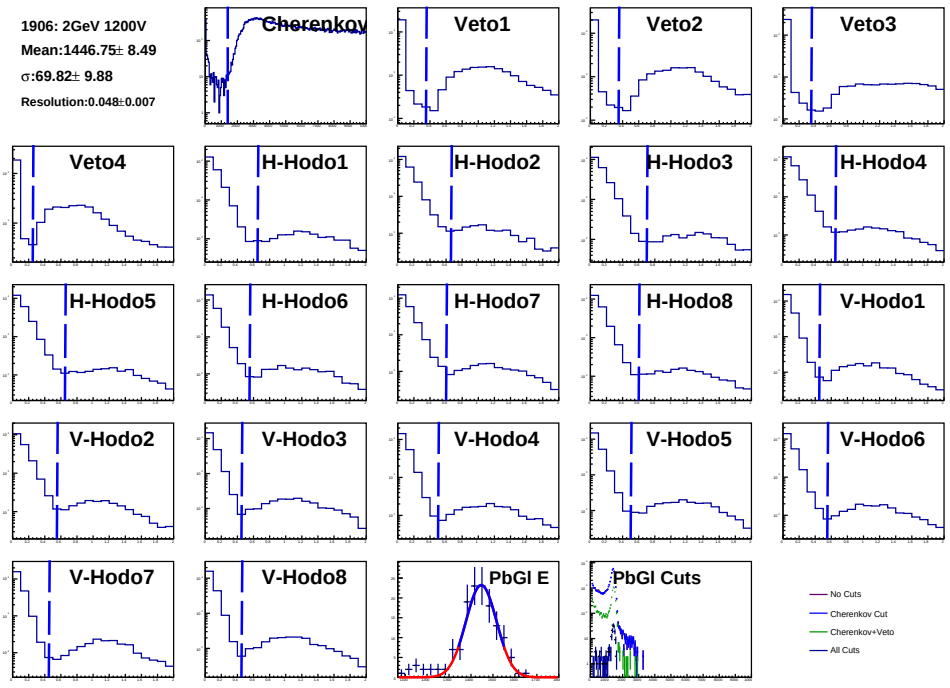

2GeV 1200V.pdf

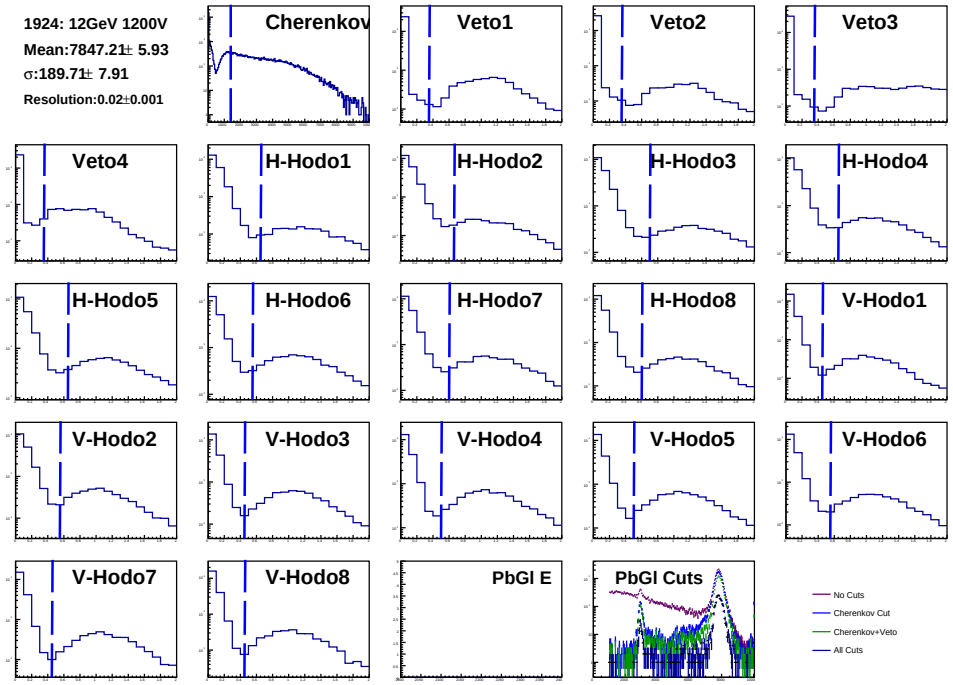

12GeV 1200V.pdf

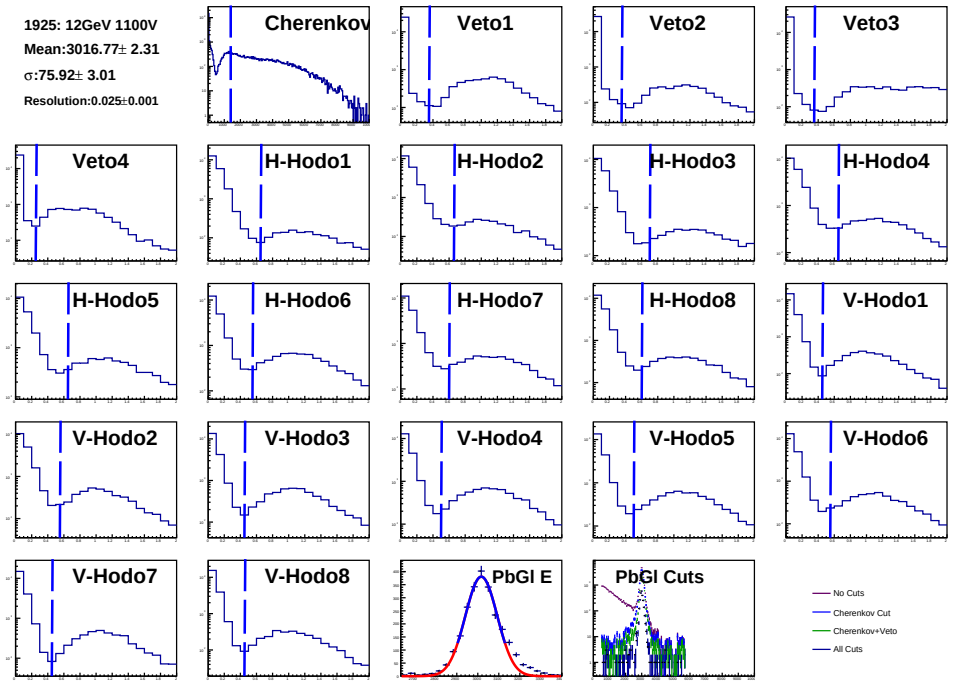

12GeV 1100V.pdf

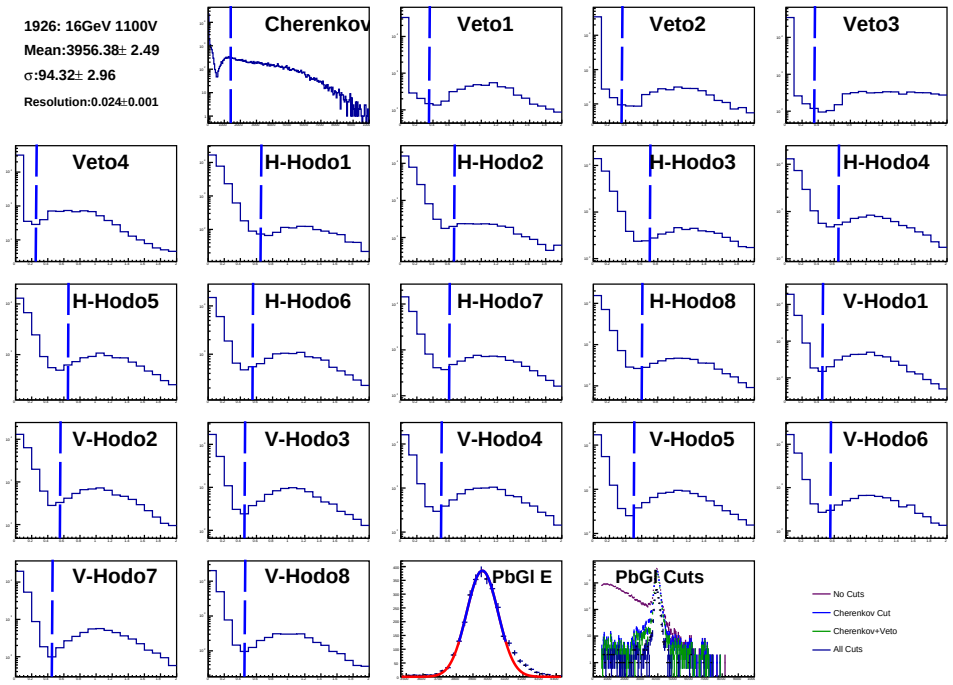

16GeV 1100V.pdf

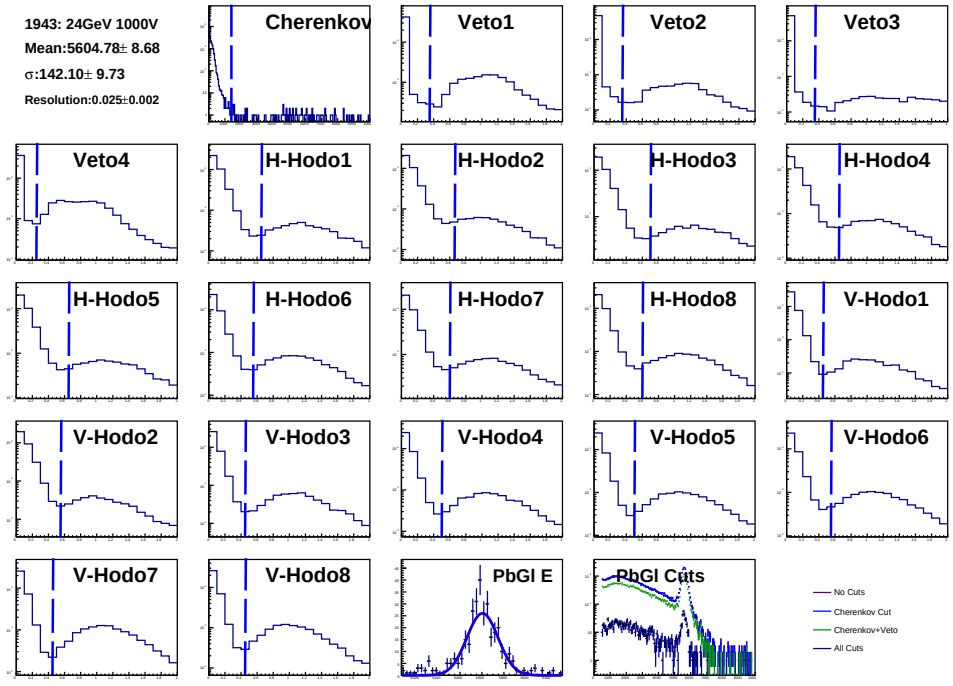

24GeV 1000V.pdf

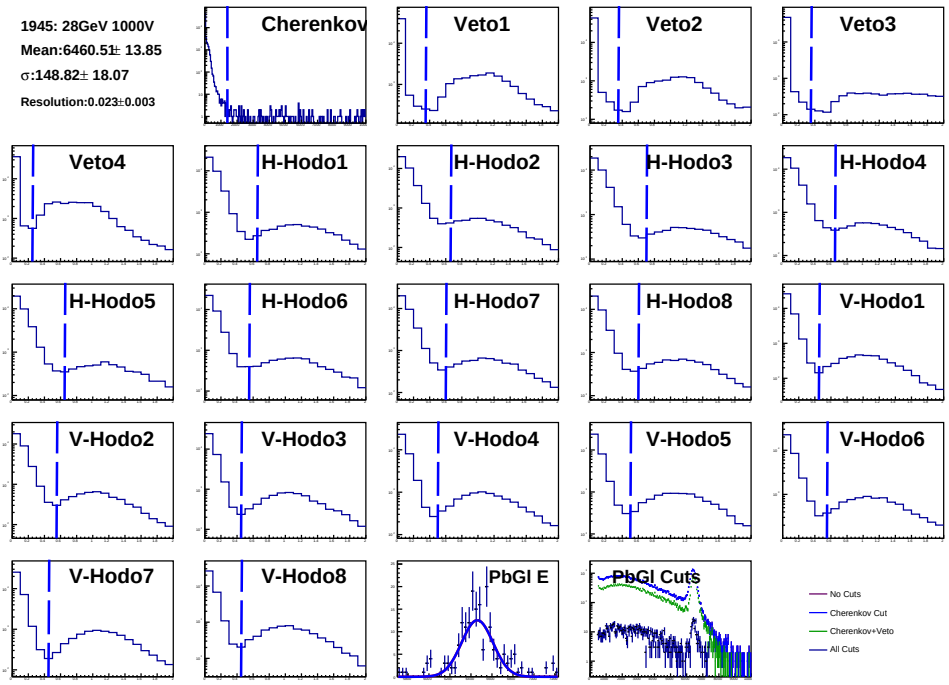

28GeV 1000V.pdf

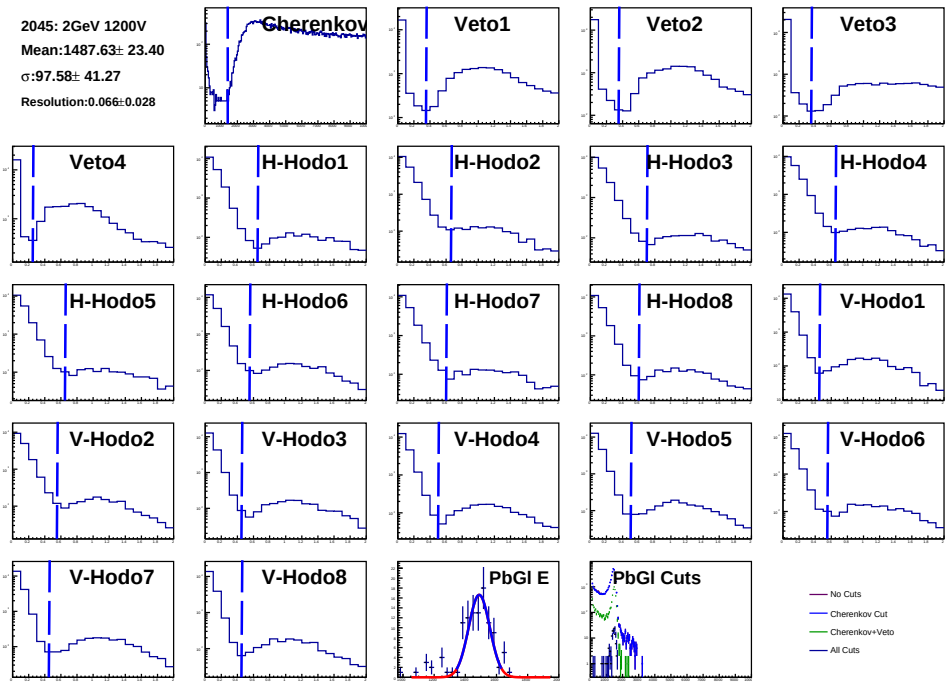

2GeV 1200V.pdf

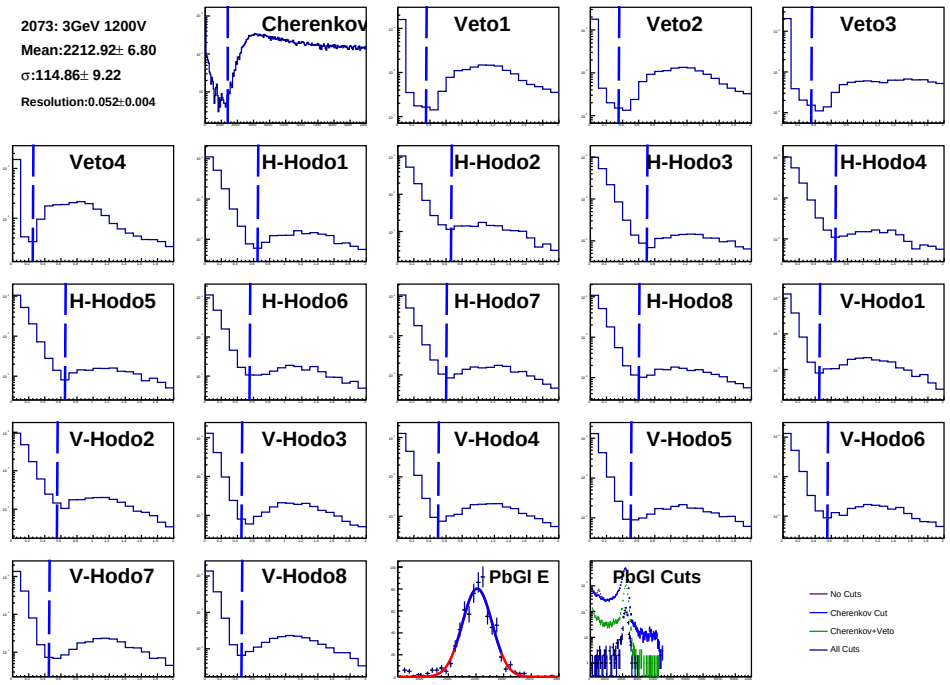

3GeV 1200V.pdf

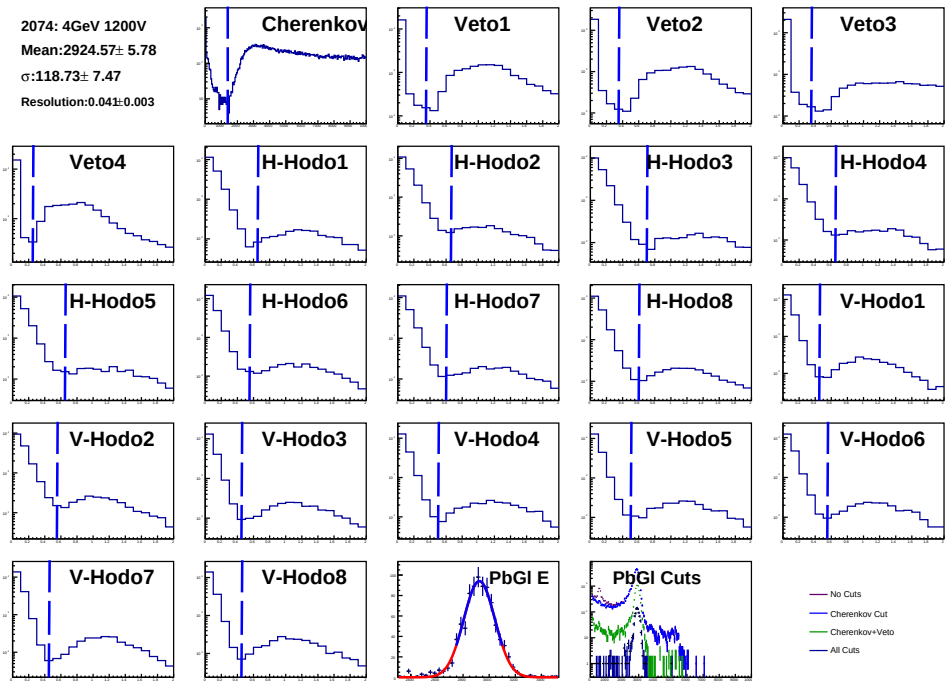

4GeV 1200V.pdf

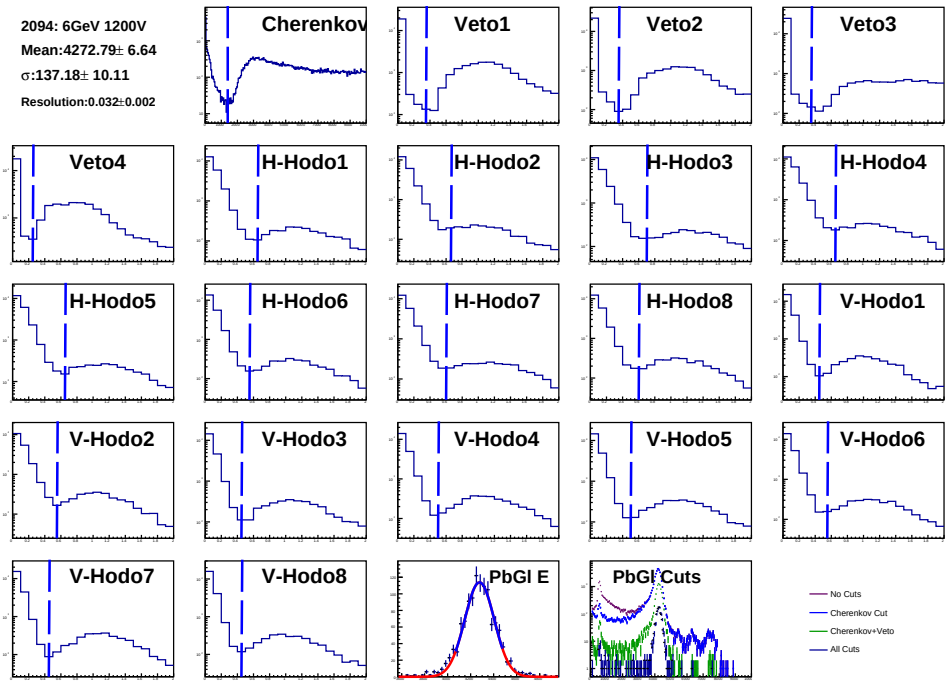

6GeV 1200V.pdf

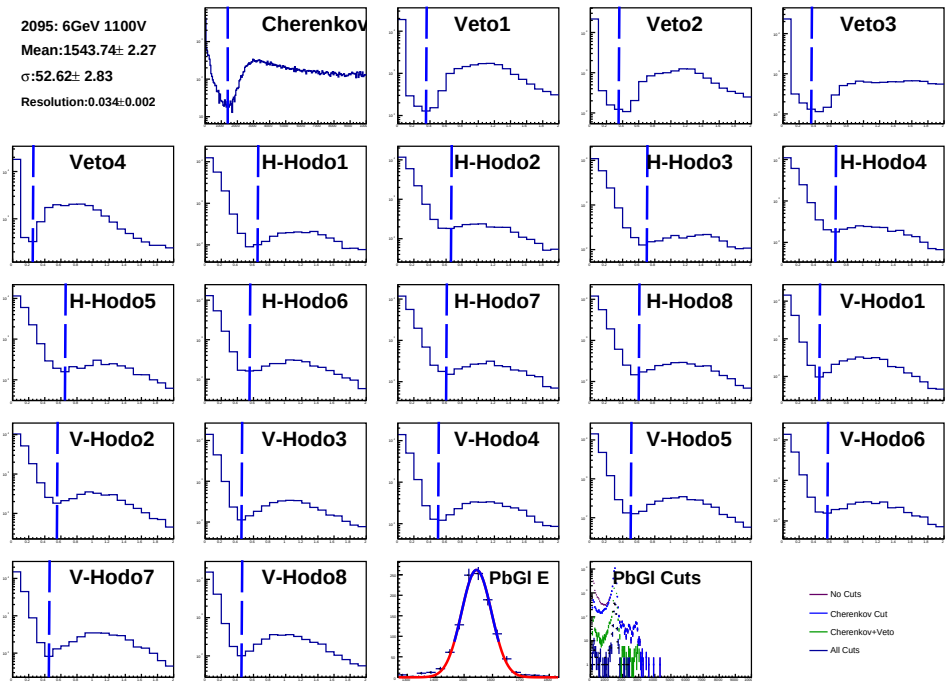

6GeV 1100V.pdf

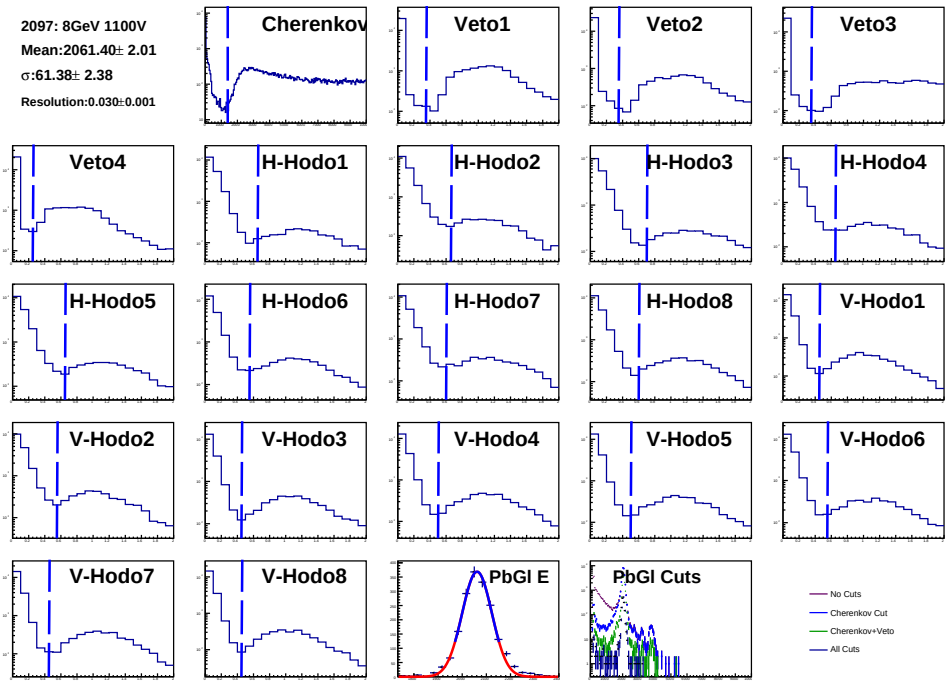

8GeV 1100V.pdf

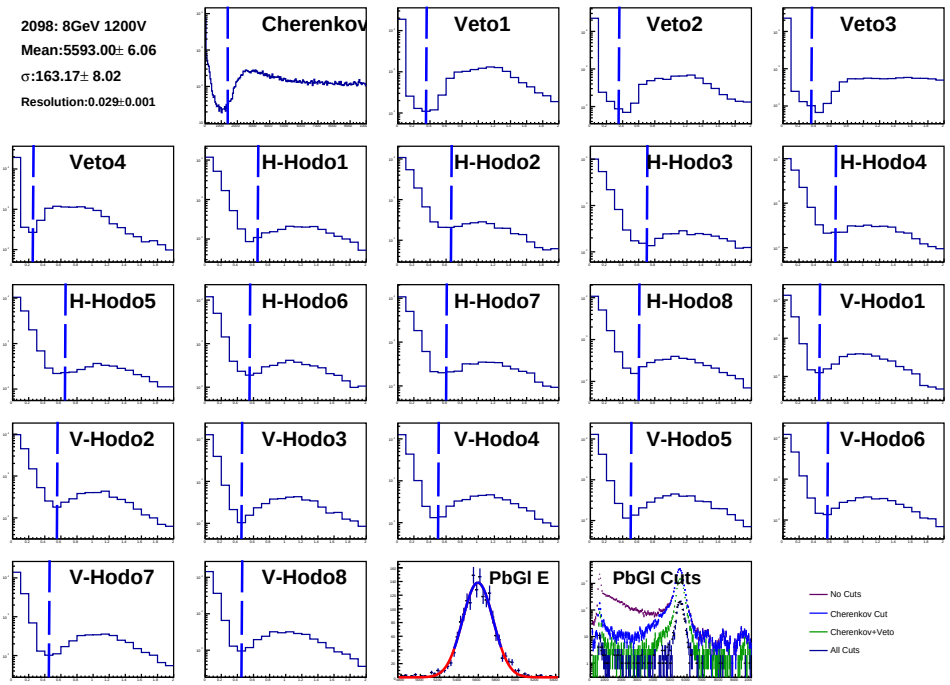

8GeV 1200V.pdf

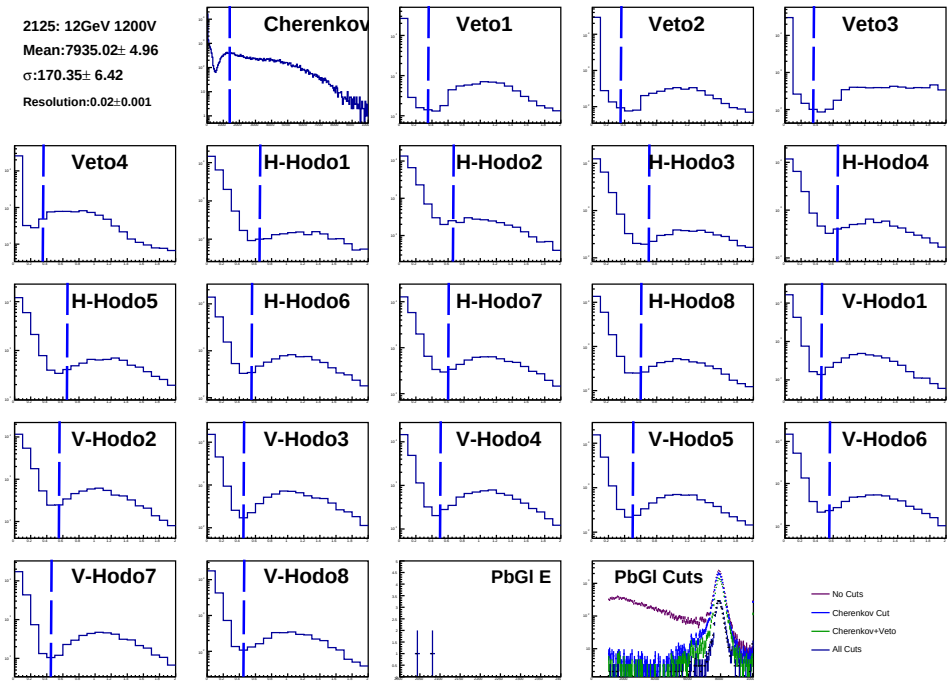

12GeV 1200V.pdf

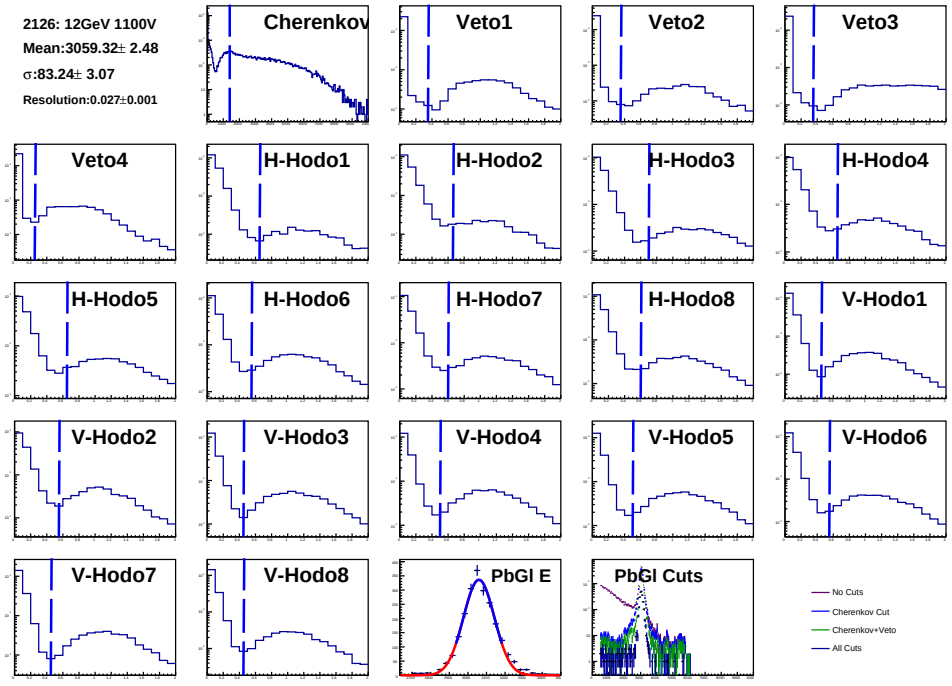

12GeV 1100V.pdf

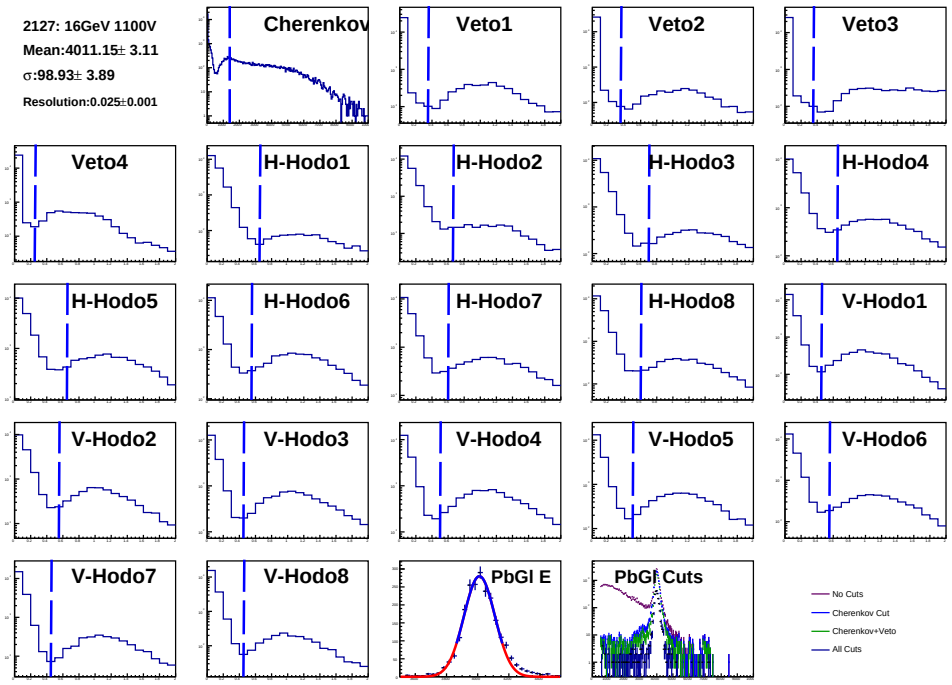

16GeV 1100V.pdf

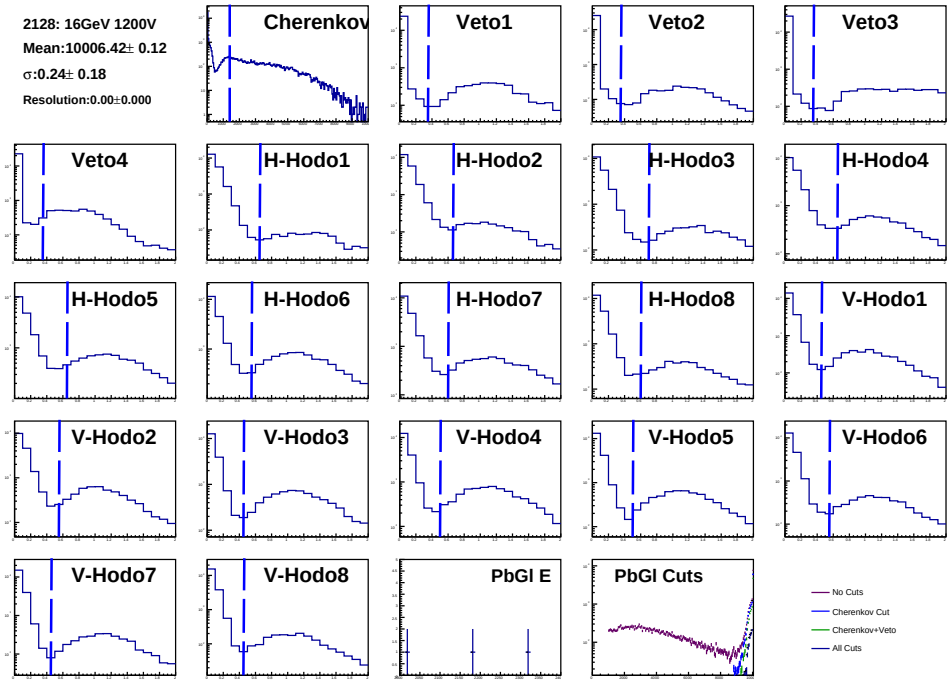

16GeV 1200V.pdf

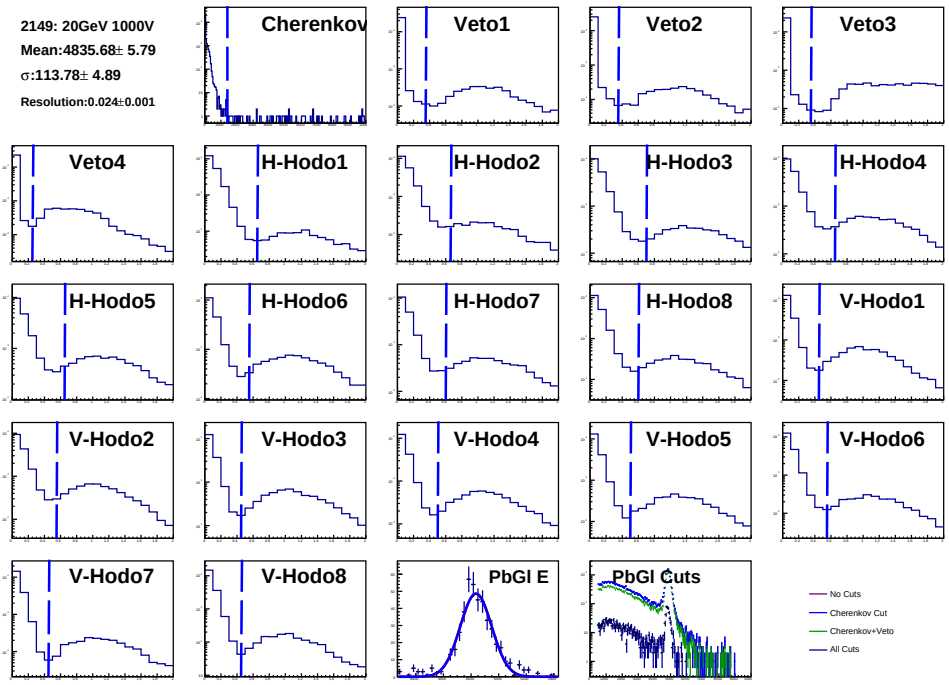

20GeV 1000V.pdf

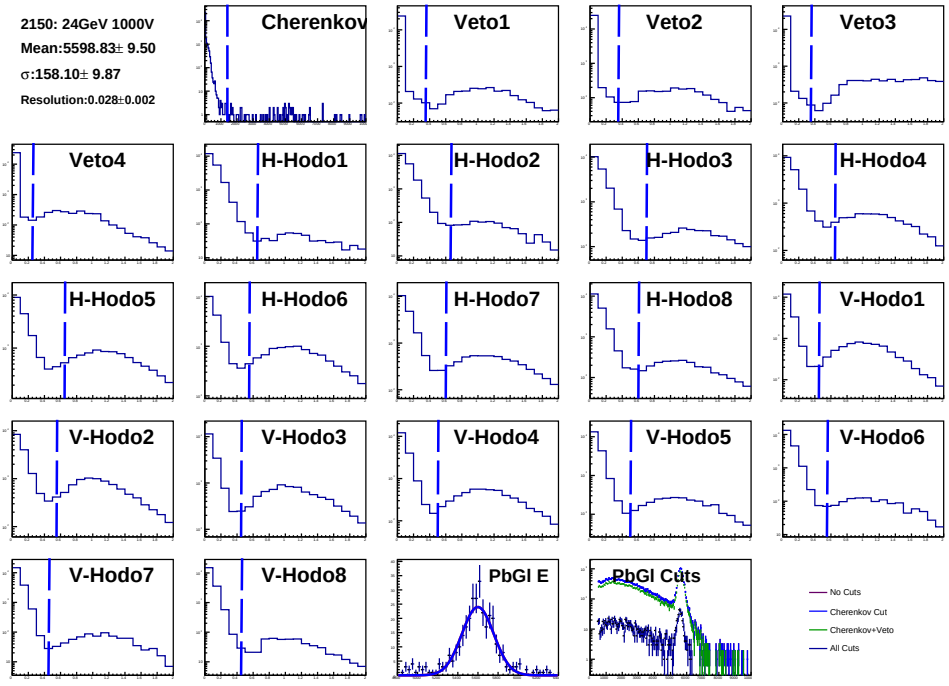

24GeV 1000V.pdf

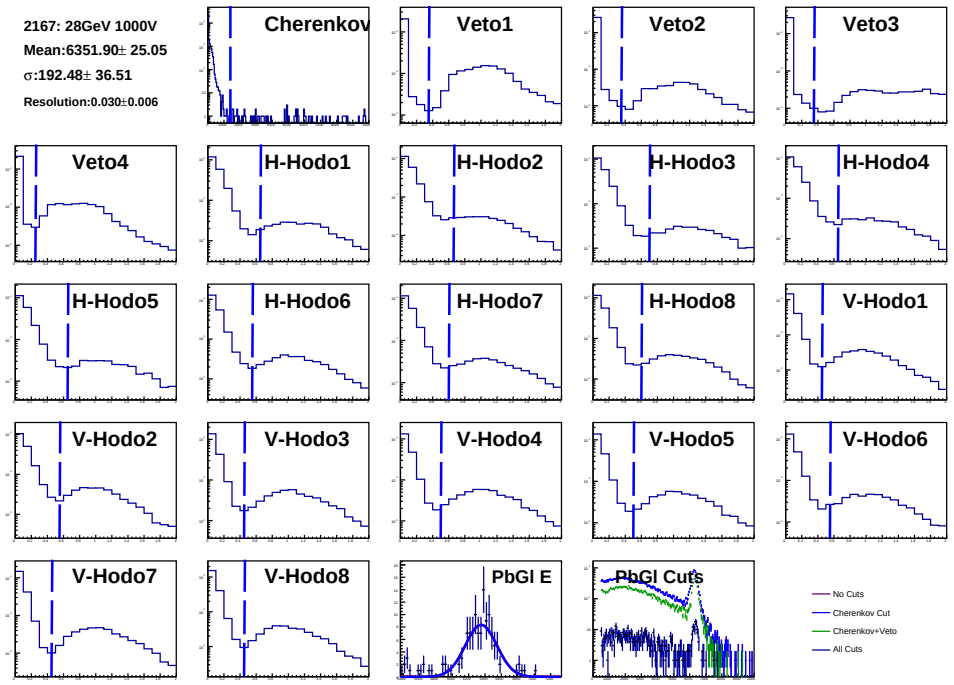

28GeV 1000V.pdf

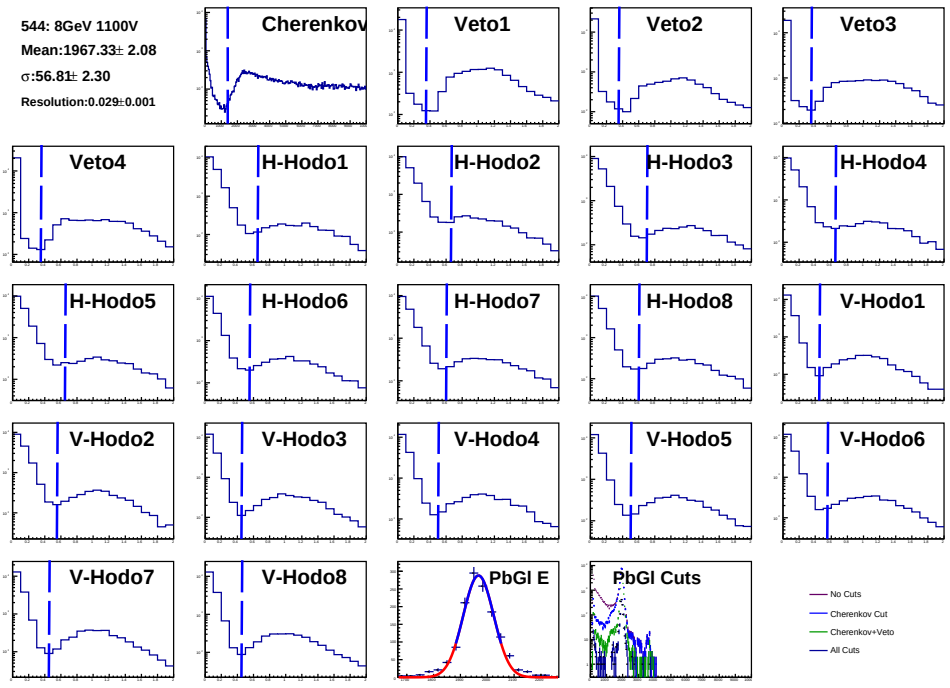

8GeV 1100V.pdf

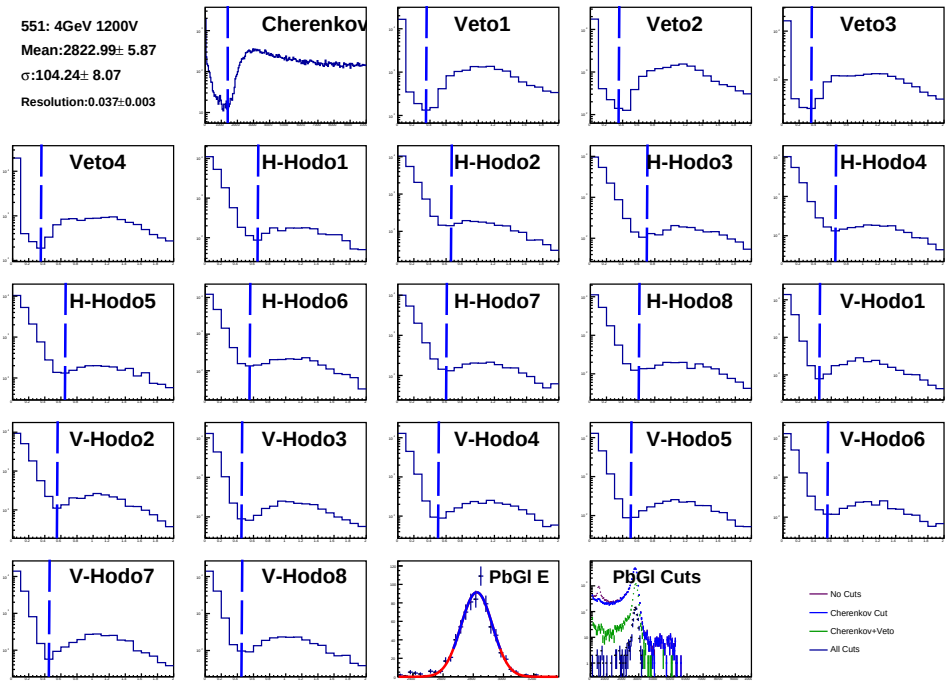

4GeV 1200V.pdf

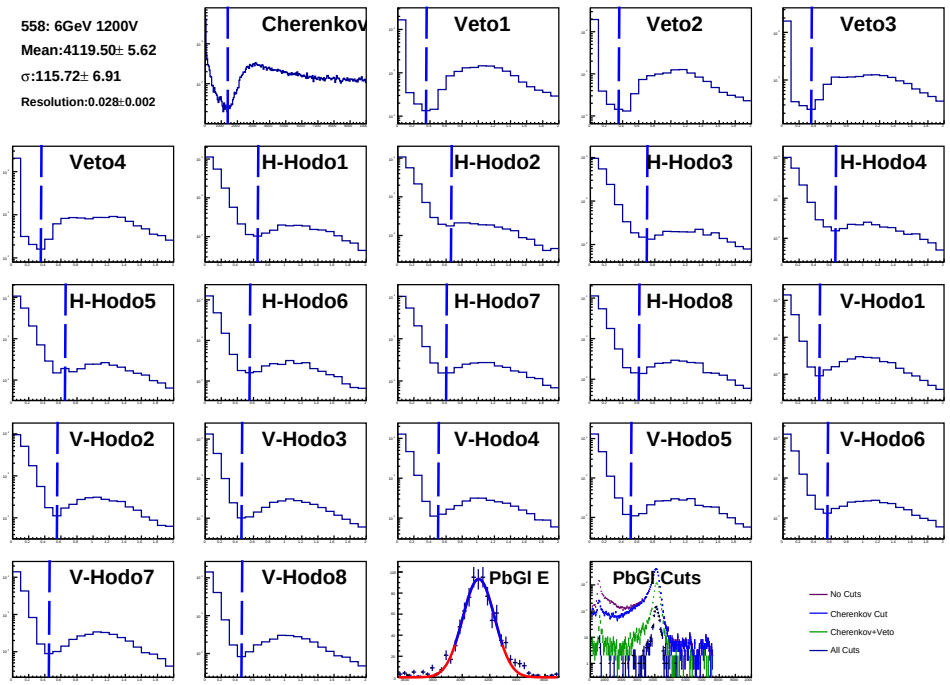

6GeV 1200V.pdf

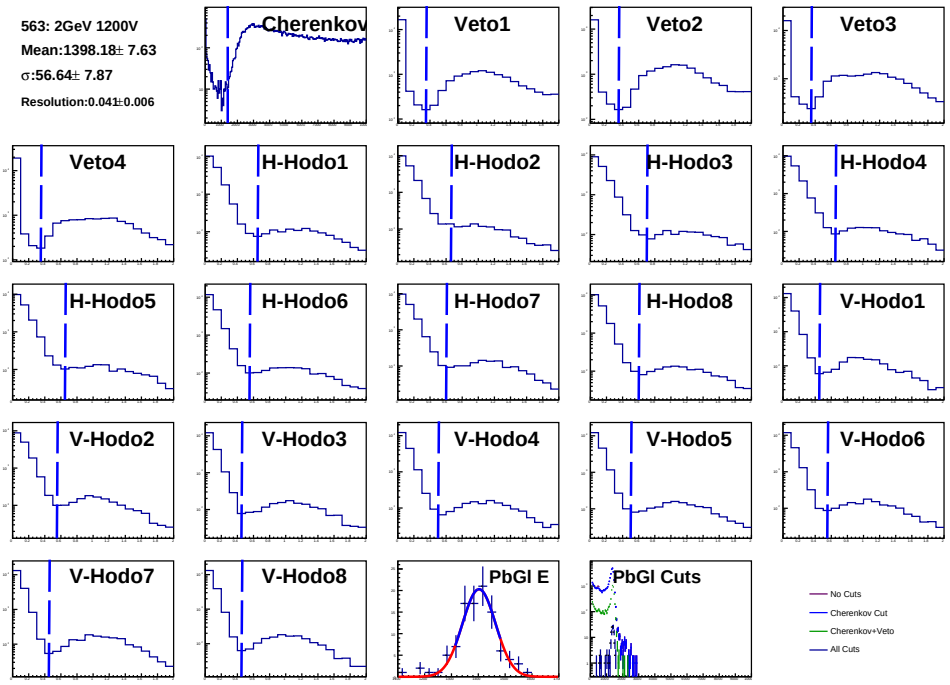

2GeV 1200V.pdf

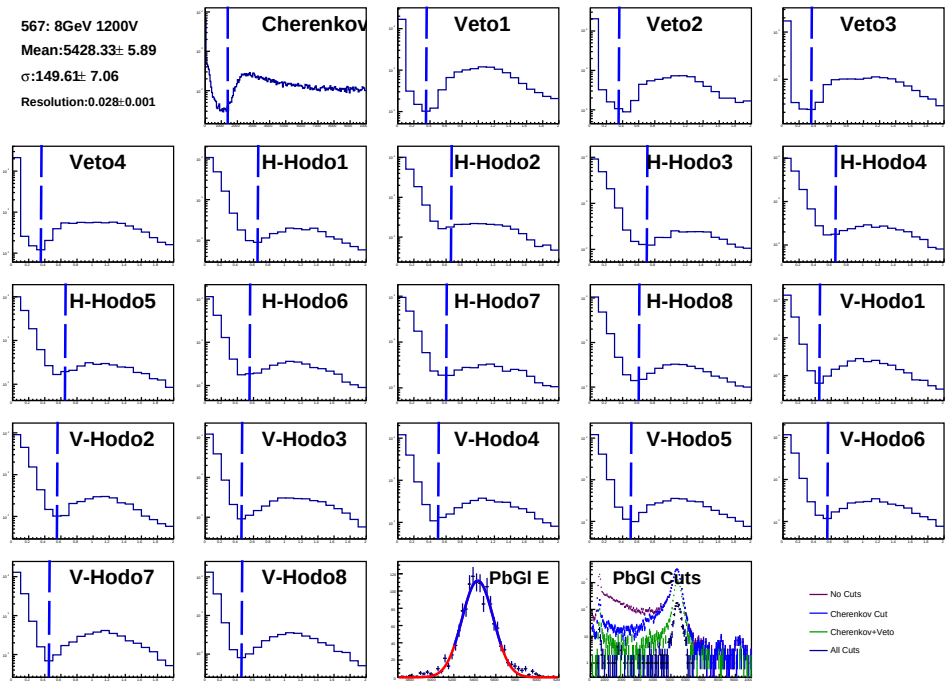

8GeV 1200V.pdf

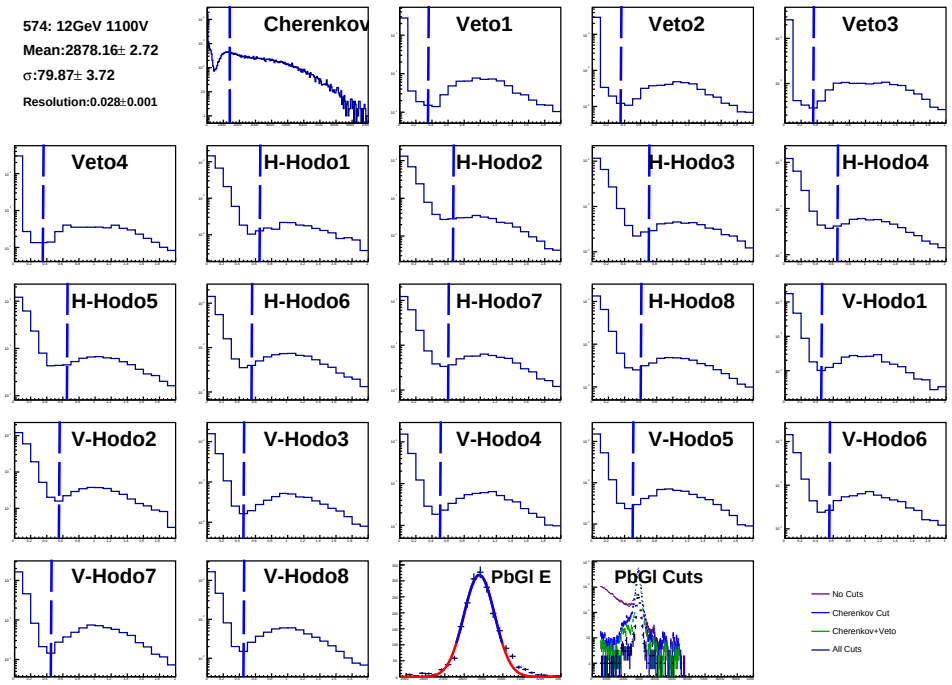

12GeV 1100V.pdf

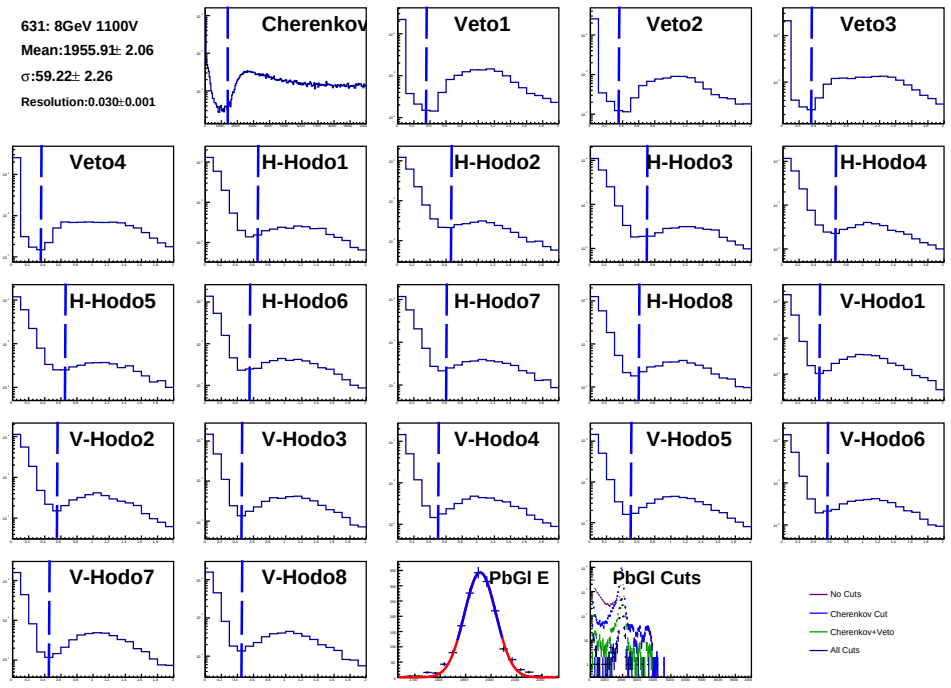

8GeV 1100V.pdf

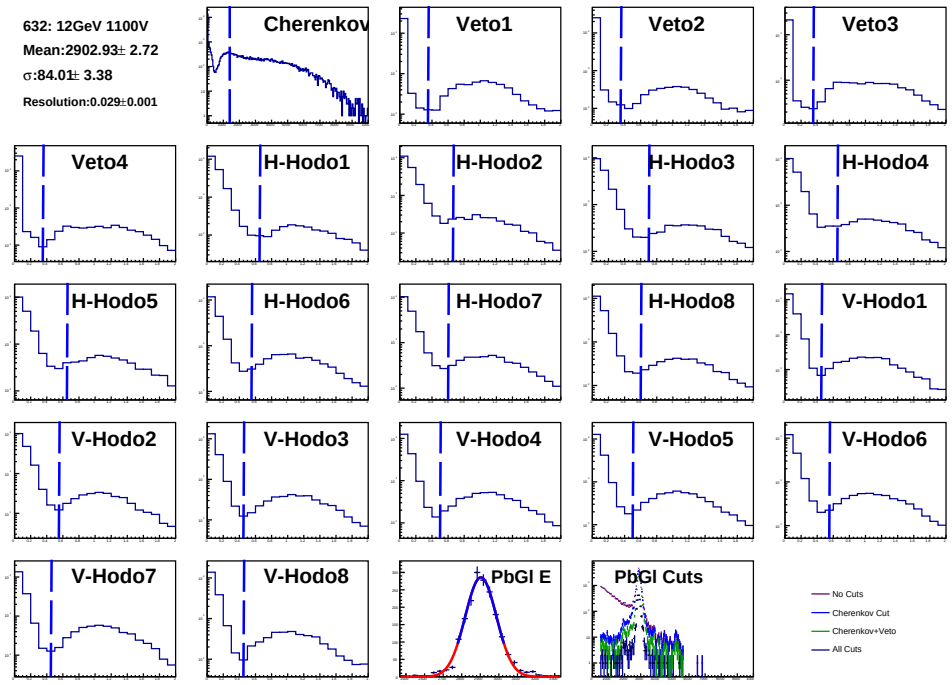

12GeV 1100V.pdf

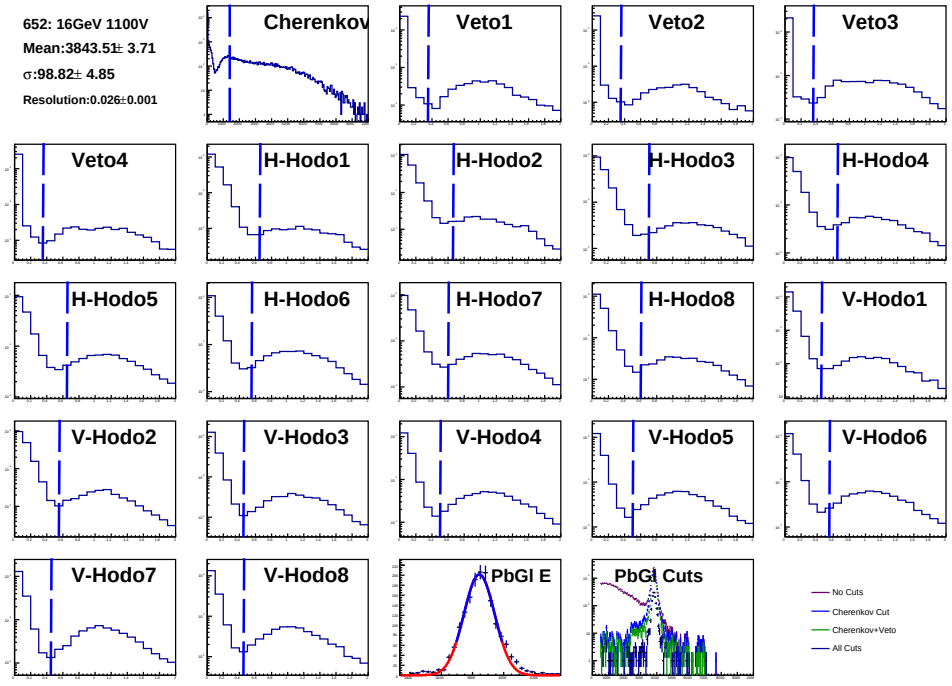

16GeV 1100V.pdf

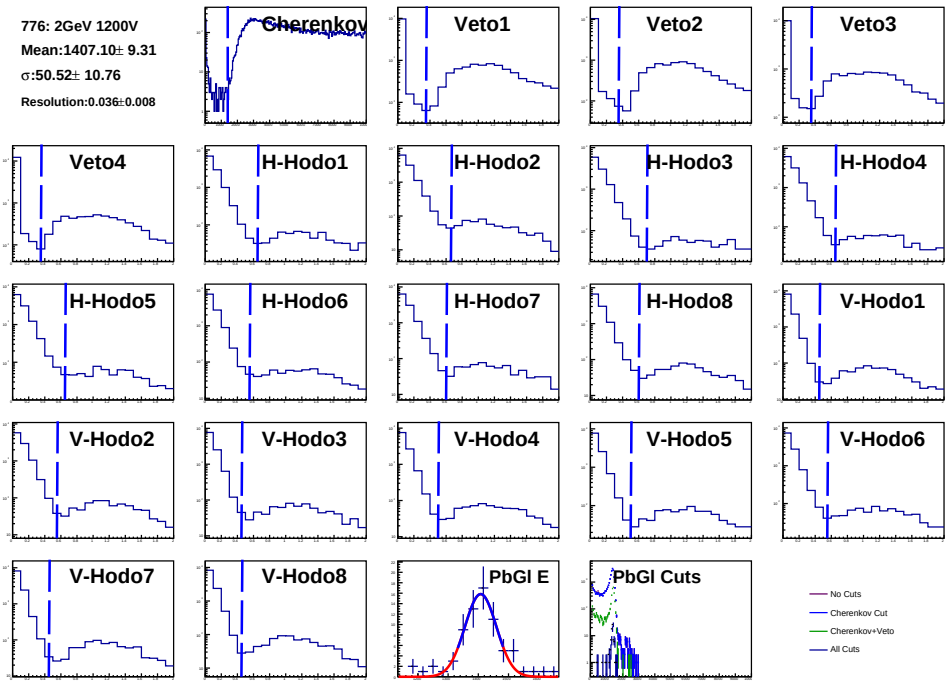

2GeV 1200V.pdf

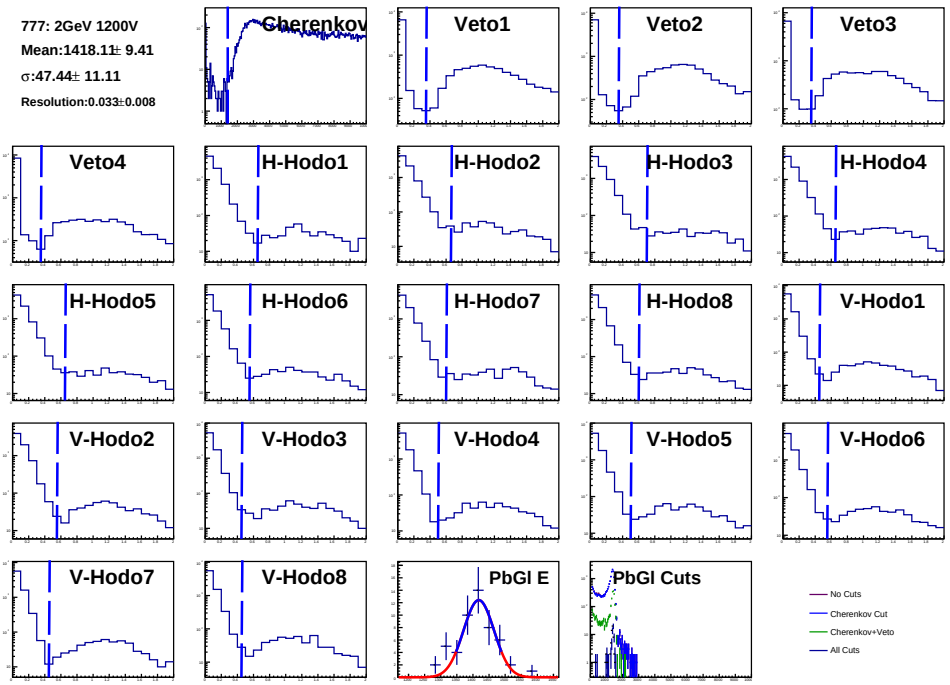

2GeV 1200V.pdf

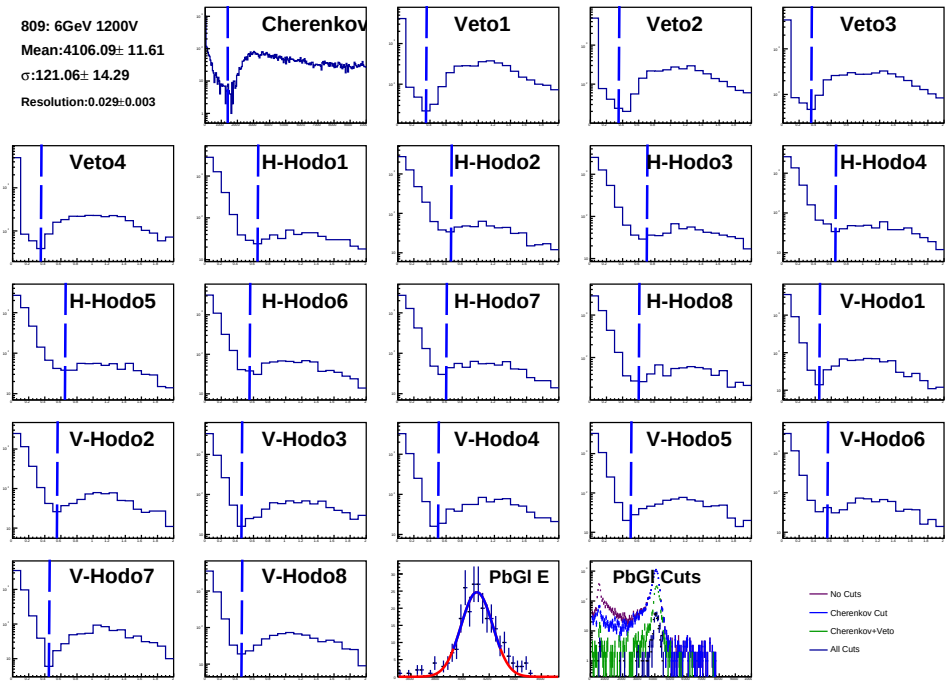

6GeV 1200V.pdf

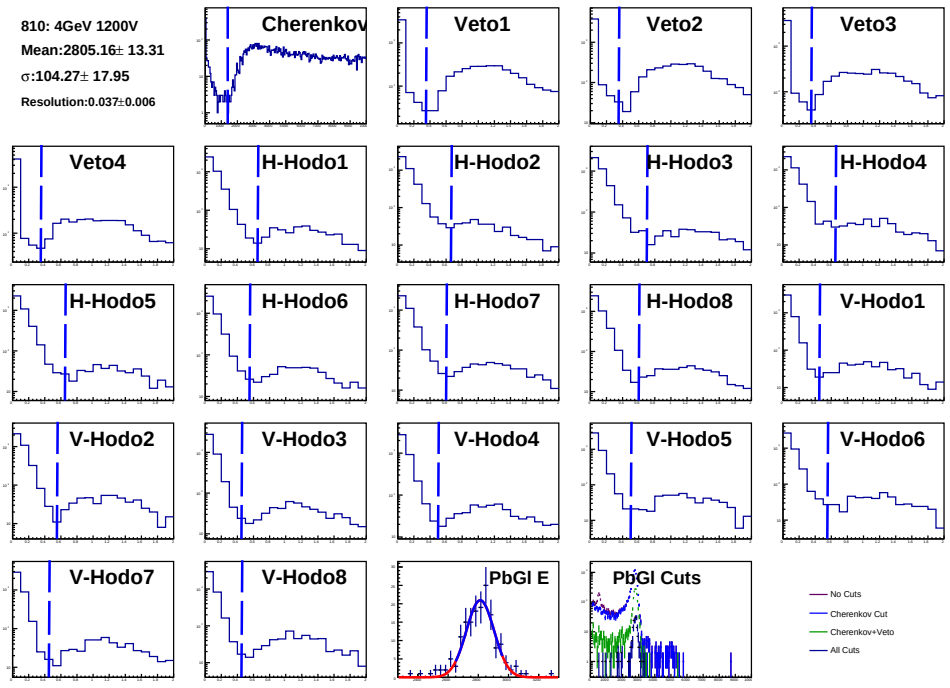

4GeV 1200V.pdf

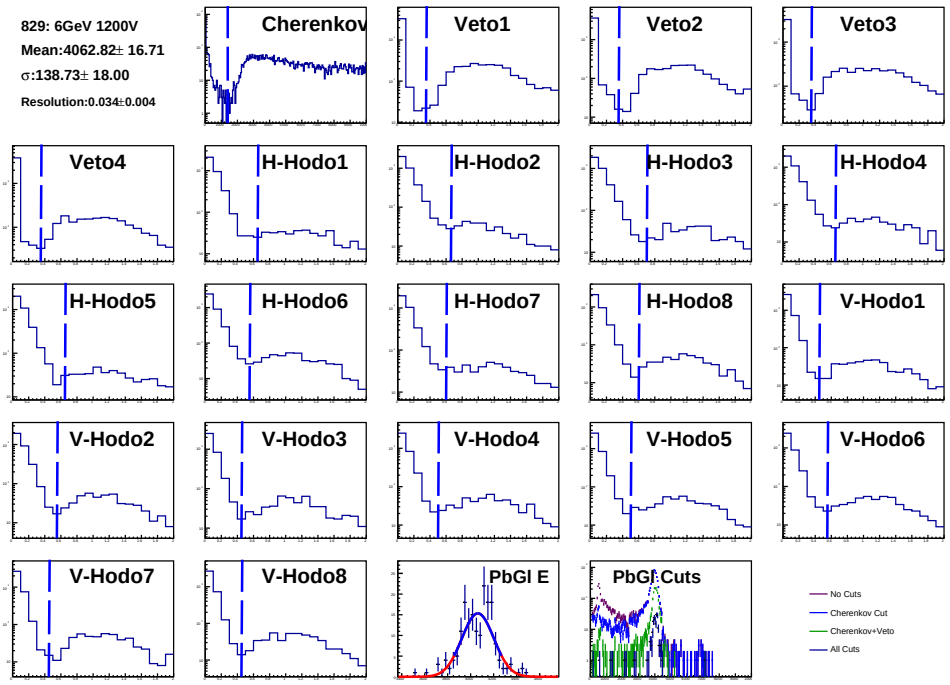

6GeV 1200V.pdf

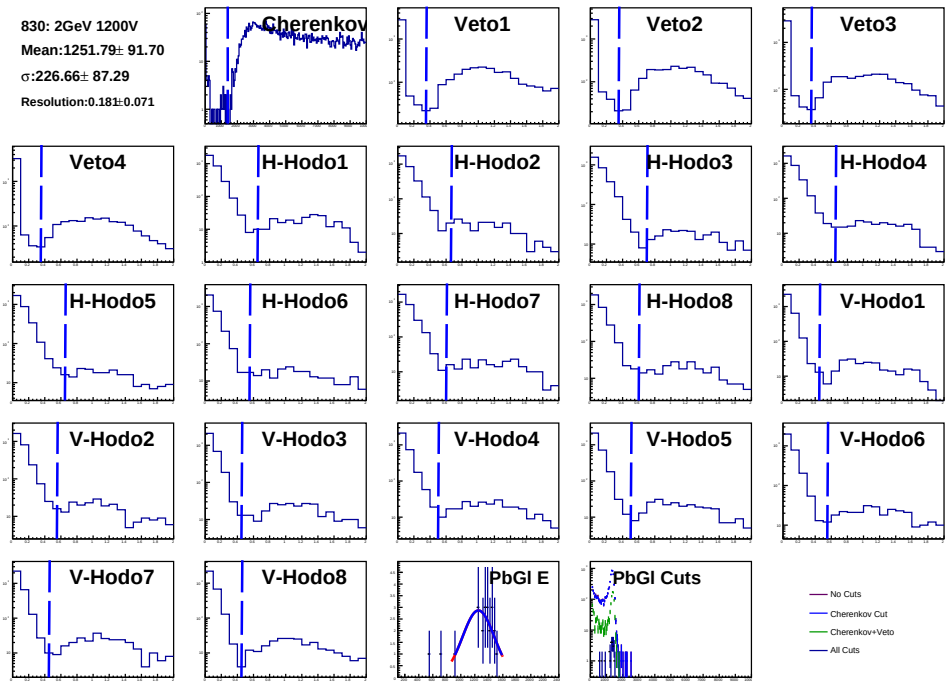

2GeV 1200V.pdf

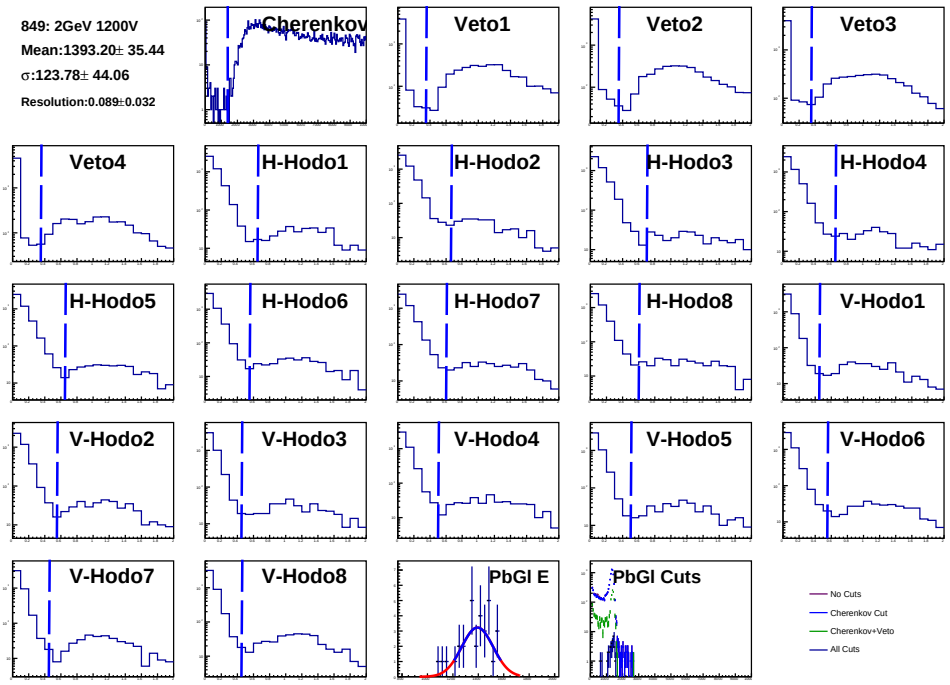

2GeV 1200V.pdf

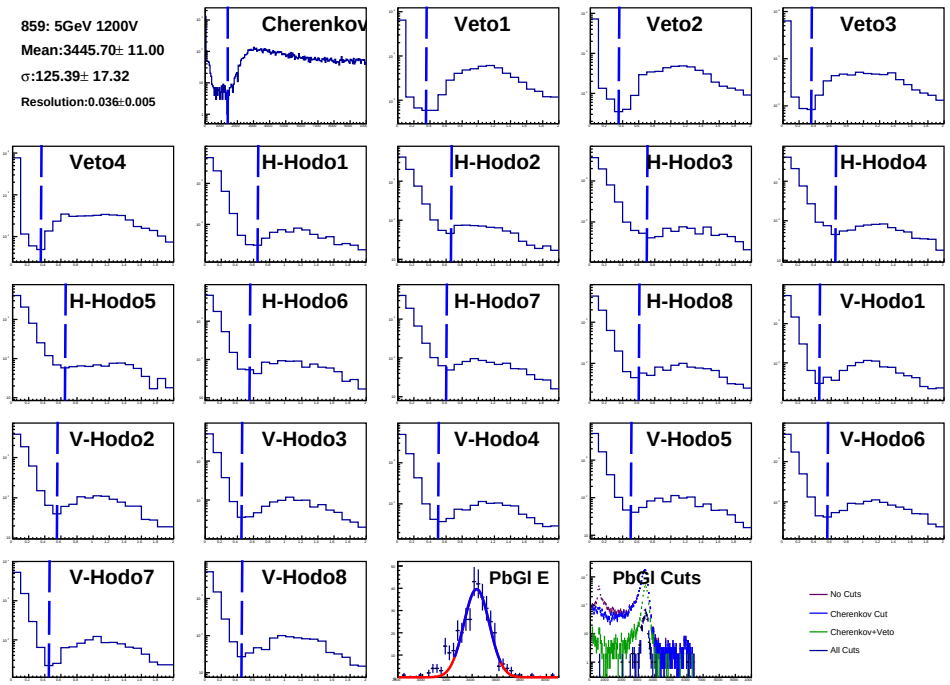

5GeV 1200V.pdf

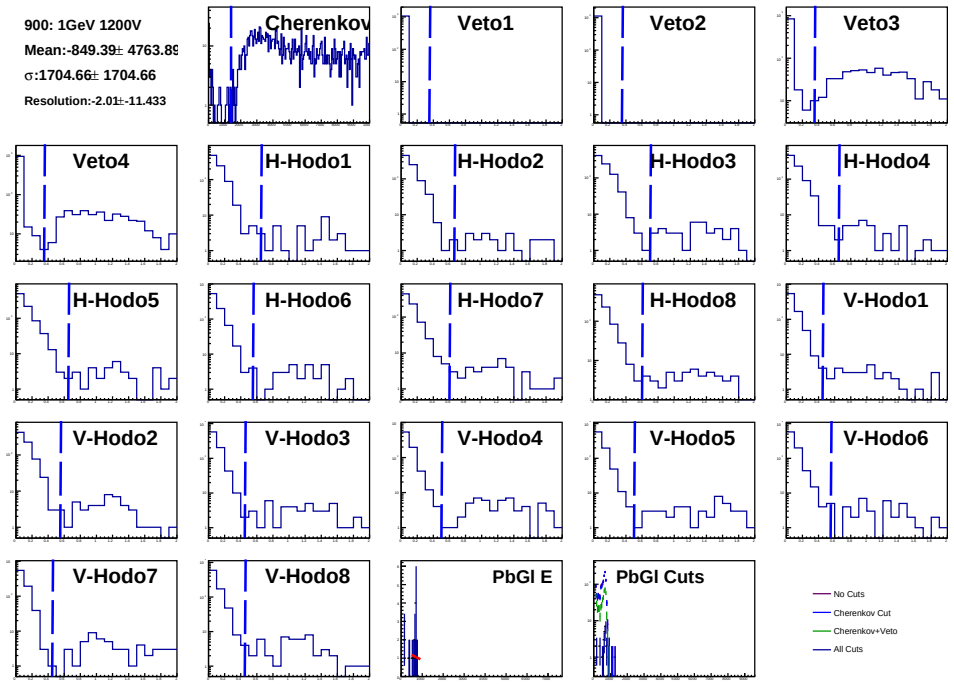

1GeV 1200V.pdf

4.4 π^- Background Model for High Energy Runs

A Gaussian background model is used to subtract the π^- background from the PbGl signal in the runs where the beam energy is greater than 20. The background is primarily π^- in this energy regime as demonstrated in figure 1.1. The Cherenkov cut is not used here due to signal like figure 1.3.

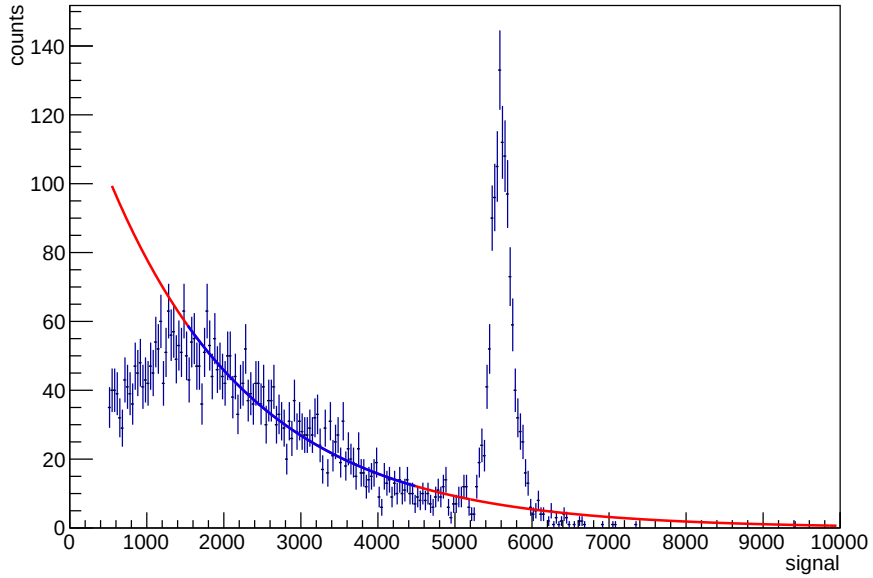

Figure 4.6: The exponential background model for run 1943.

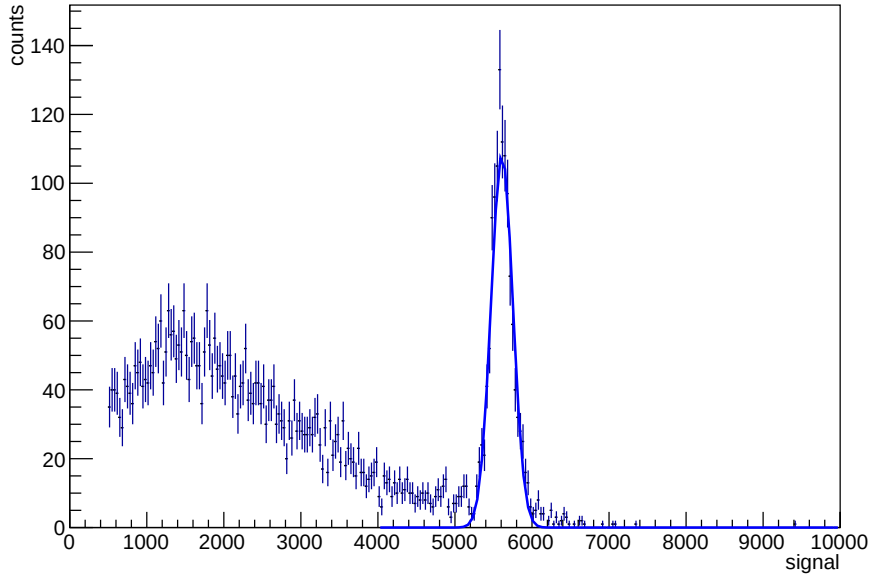

Figure 4.7: Either model yields a subtracted PbGl signal that agrees with each other. The plot above shows the Gaussian fit to the subtracted signal overlaid on the original signal.

Bibliography

[1] The fermilab test beam facility. *[online] http://ftbf.fnal.gov/*. 1.1, 1.1.2

[2] C. A. Aidala et al. Design and Beam Test Results for the sPHENIX Electromagnetic and Hadronic Calorimeter Prototypes. *Submitted to: IEEE Trans. Nucl. Sci.*, 2017. (document), 1.1.2, 2.3, 3.2

[3] C. A. M.Backfish et al. Meson test beam momentum selection. 2016. (document), 3.2

[4] R.-Y. Zhu et al. Particle Detectors at Acclerators. 2018. 3.1, 3.2